MODELING OF AGGLOMERATE ABRASION IN FLUIDIZED BEDS

by

Karthikeyan Palanisamy

B.Tech, Indian Institute of Technology Bhubaneswar, 2013

A THESIS SUBMITTED IN PARTIAL FULFILLMENT OF

THE REQUIREMENTS FOR THE DEGREE OF

MASTER OF APPLIED SCIENCE

in

THE FACULTY OF GRADUATE AND POSTDOCTORAL STUDIES

(Mechanical Engineering)

THE UNIVERSITY OF BRITISH COLUMBIA

(Vancouver)

August 2016

Abstract

Agglomeration occurs in fluidized beds in many industrial processes. It can be a desirable phenomenon, for instance in the pharmaceutical industries, or undesirable, as when it occurs in the fluid cokers used in bitumen processing. Excessive agglomerate growth can lead to a reduced efficiency of the process and ultimately to defluidization. Mathematical modeling can provide insights into agglomerate formation and breakage. Modeling the physics of agglomerate breakage is complicated since the breakage model needs to account for a number of processes occurring inside the fluidized bed. Breakage of agglomerates can happen due to fragmentation (high energy based) or abrasion (low energy based), or a combination of both. Abrasion is the process of losing one or a few of the particles from the surface of the agglomerate. It occurs continuously inside the fluidized beds and cannot be neglected for fluid cokers. Fragmentation, on the other hand, is the fracture of an agglomerate into pieces due to the breakage of multiple bonds inside it.

In this work, a physical model that describes abrasion is derived utilizing the concepts of kinetic theory of granular flows (KTGF). The model considers the collisions between the different solid phases—particles and agglomerates— to obtain the frequency of abrasion and mass transfer between the phases. A Eulerian-Eulerian formulation along with KTGF is used to simulate abrasion of a large agglomerate inside a fluidized bed. All the simulations were performed with commercial CFD code ANSYS Fluent 16, which was augmented by user-defined functions for different experimental conditions and different bed materials using published experimental data. The comparison between the modeling predictions and experimental results demonstrated a good qualitative agreement with some quantitative variations. It was found that the model tends to

underestimate the amount of abrasion for a capillary dominant system possibly due to neglecting the fragmentation phenomenon in the model. Also the model over predicts abrasion for viscous dominant set up. At the end, a mechanistic approach is suggested for future modeling of agglomerate fragmentation.

Preface

I was responsible for developing the abrasion model at The University of British Columbia with the help of my supervisors. The model development described in Chapter 3 was coded as User Defined Functions (UDF) in ANSYS Fluent and compared with the results published by Dr. Sarah Weber from the University of Western Ontario.

Table of Contents

List of Tables

List of Figures

List of Symbols and Abbreviations

A_{pa}	Area of collision plane, m^2
C_D	Drag coefficient, [-]
C_s	Fluctuation velocity, m/s
c_s	Granular velocity, m/s
Ca	Capillary number, [-]
d_p	Particle diameter, m
D	Diameter, m
$\widetilde{D}$	Non-dimensional distance, [-]
e	Coefficient of restitution for particle agglomerate collisions, [-]
E	Energy required to break a bond, J
E_m	Elasticity modulus, Pa
E_{θ_s}	Fluctuation energy, J/kg
F_d	Force of drag, N
F_g	Force of gravity, N
F_b	Force of buoyancy, N
$\vec{F}_{lift,g}$	Lift force, N
$\vec{F}_{vm}$	Virtual mass force, N
$\vec{g}$	Gravitational acceleration, m/s^2
g_0	Radial distribution function, [-]

$\bar{\bar{I}}$	Identity matrix, [-]
I_{2D}	Second invariant of deviatoric stress tensor, [-]
J	Momentum exchange between phases, kg.m/s
KE	Kinetic energy, J
KE'	Kinetic energy after collision, J
K_{sg}	Momentum exchange coefficient, $\mathrm{kg/m^3.s}$
K_c	Coordination number, [-]
k_{θ_s}	Diffusion coefficient for granular energy, $\mathrm{kg/m.s}$
m	Mass of granule, kg
$\dot{m}_{ij}$	Rate of mass transfer between phases, $\mathrm{kg/m^3.s}$
Δm	Momentum exchange per collision, kg.m/s
M_{ap}	Mass transfer between agglomerate and particle phases, $\mathrm{kg/m^3.s}$
$\dot{n}_{coll}$	Collision frequency per unit volume, $\mathrm{1/m^3.s}$
$\dot{n}_{ab}$	Abrasion frequency per unit volume, $\mathrm{1/m^3.s}$
N_b	Number of liquid bridges inside an agglomerate, [-]
N_p	Number of particles inside an agglomerate, [-]
p	Pressure, Pa
p_s	Solid pressure, Pa
P	Probability, [-]
P_{up}	Percentage underprediction, [-]
R	Radius, m
Re	Reynolds number, [-]

$\vec{R}_{sg}$ Force of interaction between phases s and g, N

S_i Mass source of ith phase, $\mathrm{kg/m^3.s}$

s Minimum separation distance between grains, m

t_c Collision time, s

Δt Time step, s

U Superficial gas velocity, m/s

U_{mf} Minimum fluidization velocity, m/s

U_s Mean velocity, m/s

$\overrightarrow{v_i}$ Velocity field vector of ith phase, m/s

v_i Velocity field scalar of ith phase, m/s

$\hat{v}_i$ Unit vector along direction of v_i, m/s

$\vec{v}_{sg}$ Relative velocity between phases s and g, m/s

$\vec{v}'$ Velocity after collision, m/s

V Volume, $\mathrm{m^3}$

$\tilde{V}$ Non dimensional volume, [-]

$\vec{V}_r$ Relative velocity of spheres, m/s

Greek Letters

ε Volume fraction, [-]

$\varepsilon_{s,max}$ Packing limit, [-]

ρ Density, $\mathrm{kg/m^3}$

θ_s	Solid phase granular temperature, J/kg
θ	Contact angle between particle and binder, °
μ	Shear viscosity of gas phase, kg/m.s
λ	Bulk viscosity of gas phase, kg/m.s
$\bar{\bar{\tau}}$	Stress tensor of gas phase, Pa
τ	Relaxation time of a phase, s
Γ	Interface energy, J/m^3
φ	Angle of internal friction between grains, °
φ_{ps}	Transfer of kinetic energy, kg/m.s^3
γ_{θ_s}	Collisional dissipation energy, kg/m.s^3

Abbreviations

2D	2 Dimensional
3D	3 Dimensional
CFD	Computational Fluid Dynamics
$C.N$	Coordination Number
DNS	Direct Numerical Simulations
FCC	Fluid Catalytic Cracking (FCC)
KTGF	Kinetic Theory of Granular Flows
PDE	Partial Differential Equation
PBE	Population Balance Equation
PBM	Population Balance Model

Subscripts

a	Agglomerate Phase
ab	Abrasion
b	Bond
c	Collision
col	Collisional
co	Coordination
cap	Capillary
fr	Fragmentation
fric	Frictional
g	Gas Phase
geom	Geometric
kin	Kinetic
p	Particle Phase
r	Ratio
s	Solid Phase
visc	Viscous

Acknowledgements

I would like to express my very sincere gratitude to my supervisors, Professor Martha Salcudean and Professor Dana Grecov, for providing me with the opportunity to work on this project of interest. I feel extremely grateful for their endless support academically and personally. I would like to sincerely thank them for being patient during my graduate studies and for allowing me to take time off to attend important family events. I feel very fortunate and blessed to have worked under their guidance.

I express my gratitude to Dr. Konstantin Pougatch for his time, help and advice on my path to enlarge my vision of science and for providing coherent answers to my questions. I would like to thank Dr. Amir Motlagh for the weekly meetings and for helping me with my research questions, which guided me to reach my research goals.

Also, I would like to acknowledge the financial support provided by NSERC (Natural Sciences and Engineering Research Council) and Syncrude Canada Ltd. I am also very grateful to my friends Subodh, Harshmeet, Nick, Mohammad and Arian who helped me with their valuable suggestions and support during my stay at our research lab. Special thanks are owed to my parents, who have supported me throughout my years of education, both morally and financially.

Chapter 1: Introduction

1.1 Background

Canada is in third place in terms of proven global oil reserves, with an estimated potential of 339 billion barrels of crude oil resources, of which oil sands bitumen accounts for 90% (1). Bitumen is a highly viscous and dense feedstock made up of heavy hydrocarbons which require further processing to obtain synthetic crude oil. These heavy hydrocarbons need to be broken down into lighter components, which then could be used to produce more valuable products. This procedure is generally referred to as "upgrading" of heavy oils. There are two well-known methods for cracking the heavy hydrocarbons. One involves a catalytic process used in fluid catalytic cracking (FCC) reactors and the other involves a thermal cracking process used in fluid cokers (FC).

The bitumen upgrading process in fluid cokers, which are mainly operated by Syncrude Canada Ltd., is carried out in fluidized beds of coke particles where the injected liquid feed is thermally cracked after contacting heated coke particles. Figure 1.1 shows the schematic representation of a fluid coker. The coke particles are fluidized using steam flow, and bitumen is injected through nozzles using steam-assisted atomization. In the process of cracking, heat is transferred from the coke particles to the bitumen and the coke particles cool down. They are then reheated in a burner and reintroduced into the fluidized bed.

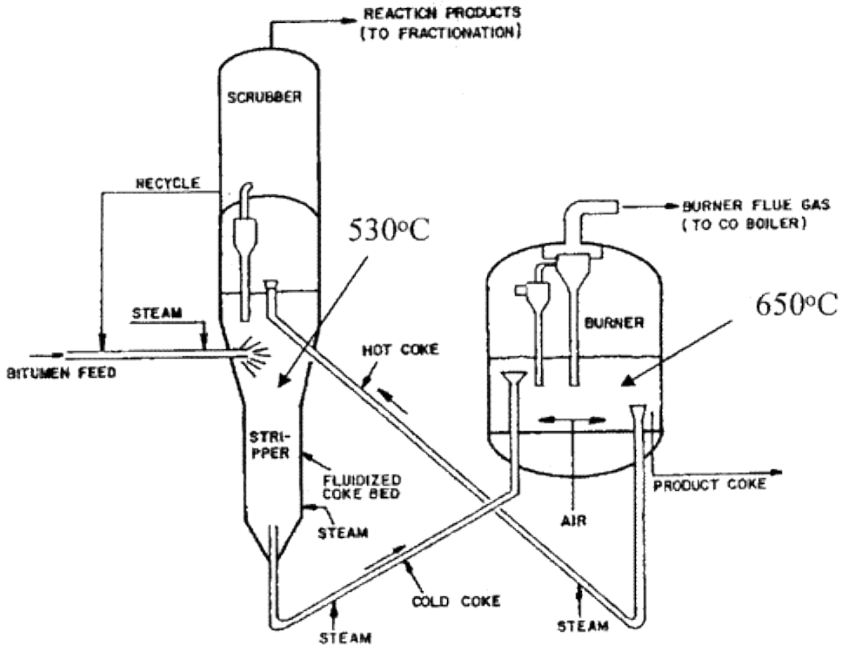

Figure 1.1: Schematic representation of a fluid coking system (House et al. (2))

1.2 Motivation

Due to improper mixing of coke particles and bitumen, some particles carry high bitumen content in their coating, which results in the formation and growth of agglomerates in fluid cokers (3, 4). Agglomerates are defined as groups of individual solid particles held together by the binding effect of the liquid. Over time, agglomerates with hundreds of coke particles are formed. This is undesirable because their formation can lead to reduced process efficiency and possible defluidization of the fluid cokers. Agglomerates lead to reduced heat transfer and lower product yields. As well as agglomerate growth, breakage of agglomerates also occurs either due to internal processes such as collisions or solid drag, or due to external forces like high-speed steam jets. In view of the importance of fluid cokers in oil refineries, a better understanding of the agglomerate breakage processes is crucial in order to better understand the underlying

physics of agglomeration. The main objective of this thesis is to shed light on the complexities of the breakage phenomenon and to propose an approach to enhance modeling of agglomerate breakage.

1.3 Literature Review

There are two types of collisions in which the surfaces of particles make contact: dry and wet collisions. For dry collisions, particle-particle contact can be modeled based on consideration of forces acting on and between dry particles, which are drag, gravity, buoyancy, collision and inter-particle cohesive forces (e.g., van der Waals force). The buoyancy force is usually neglected due to the large difference between fluid and particle densities. The collision force in dry contact is usually described by the Hertzian theory, which is based on the assumption of a flattened tip at the collision point with deformation outside the contact region (4). When wet collisions are studied, a thin layer of liquid film is considered to reside on the surface of the contacting particles. The addition of a liquid layer significantly changes the behavior of the two colliding particles. The particles may stick together as a result of the viscous liquid layer, represented as viscous force, or the formation of a liquid bridge between contacting particles by the capillary effect, represented as capillary force when modeling wet collisions. Seville et al. (5) reviewed all the main inter-particle forces related to fluidization and estimated that cohesive forces, e.g., van der Waals and electrostatic forces, are orders of magnitude smaller than the capillary forces. Therefore, for the range of particle dimensions investigated in this study, cohesive forces are usually ignored when studying wet collisions in fluidized beds. The strength of the capillary force has been the subject of extensive theoretical studies (6-8) and details on the expressions are discussed in later chapters.

1.3.1 Granulation Process

The granulation process consists of three sets of processes which are wetting and nucleation, consolidation and growth, and attrition and breakage (7).

1.3.1.1 Wetting and Nucleation

Wetting of the particles occurs when the particles come in contact with the binder liquid, which results in the formation of a nucleus. Schaefer et al. (8) proposed that the properties of the initial nucleus depend on the difference in the size scales of the particle and binder droplet. Immersion occurs if the size of the liquid binder droplet is significantly larger than the particle size and the particles are partially or totally immersed in the liquid and have saturated pores. With smaller droplet sizes, the liquid gets distributed over the particles. When these coated particles come in contact with each other, coalescence occurs. Figure 1.2 shows the initial nucleus formation in coalescence and immersion mechanisms when the liquid comes into contact with the particles. The nucleation kinetics also depends on the binder delivery system, the degree of binder dispersion, and the extent of bed element mixing (7).

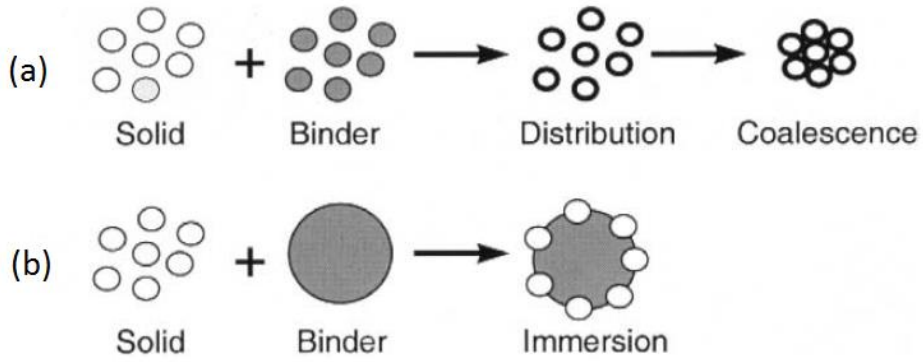

Figure 1.2: Mechanism of nucleus formation. (a) Distribution mechanism (small droplets), (b) immersion mechanism (large droplets) (Schæfer et al. (8))

1.3.1.2 Agglomerate Growth

Growth of the granules occurs when the primary particles of the bed stick to an existing nucleus due to the presence of binder coating. Growth regime maps have been proposed to study the factors that dominate the growth of agglomerates (9). These maps have limitations, as they do not consider the effects of nucleation and wetting, and they do not predict the rate and extent of the growth of agglomerates. McDougall (10) studied the effect of the liquid viscosity and contact angle on the growth mechanism. He reported that beyond the threshold values of viscosity and contact angle, the growth of agglomerates occurs even when the liquid is distributed uniformly in the bed. Rajniak et al. (11) conducted experiments to study the effect of binder content on the growth of agglomerates and concluded that with the increase in the liquid content, the agglomerates had faster growth.

1.3.1.3 Destruction of Agglomerates

Destruction of agglomerates can happen due to different phenomena such as fragmentation and abrasion. Fragmentation occurs when the agglomerates break down into a few smaller parts. Fragmentation can occur for many reasons, such as interaction with high speed jets, impact with impellers, and shear inside the bed (7). This phenomenon has a very high influence on the overall size distribution of granules and hence the efficiency of the particulate process (12, 13). Abrasion, on the other hand, is the process of losing particles from the surface of the agglomerate. It needs low energy for abrasion compared to fragmentation, as only a few bonds need to be broken. Though the loss of a few particles from an agglomerate might not affect the effective size of the agglomerate, abrasion occurs continuously inside fluidized beds. Hence, its

overall effect can be quite significant as the agglomerates can abrade completely (14). Figure 1.3 shows a schematic representation of fragmentation and abrasion in agglomerates.

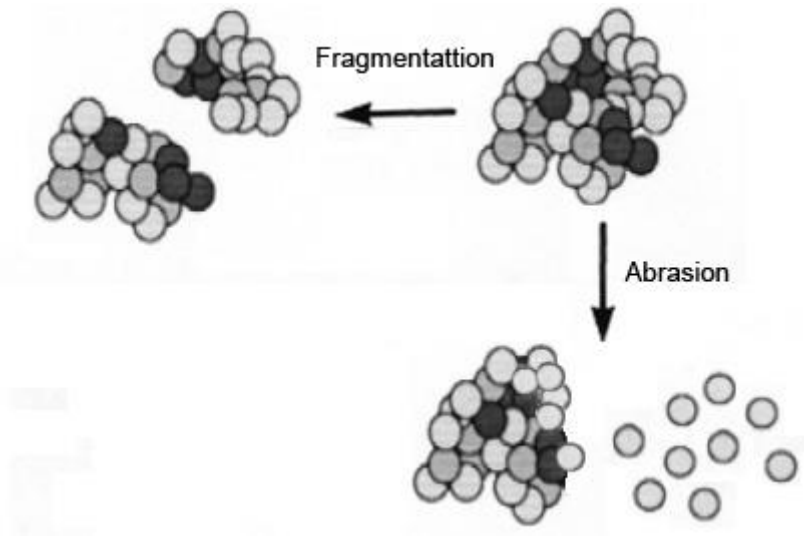

Figure 1.3 : Destruction mechanism of agglomerates (Vonk et al. (15))

1.3.2 Strength of Agglomerates

The primary particles, which constitute the agglomerate, are bound together through many internal forces. These forces could arise due to the physical or chemical properties of particles, and their range can be very small. Also, the forces can arise either due to some reactions occurring inside the agglomerates or due to the sticking force of some external binder that forms bridges between the particles (16). The scope of this thesis is to study abrasion in liquid-solid agglomerates in which an external binder forms liquid bridges that hold the primary particles together.

The importance of the liquid between the particles in the agglomerate depends on the amount and properties of liquid binder (17). At lower amounts of liquid binder, pendular bridges are formed where liquid connects two particles at their surface points. The strength of the agglomerate at this saturation level is due to the formation of liquid bridges. As the amount of liquid binder increases, it fills some of the pore spaces in the agglomerate, reaching the funicular state. With further increase in the binder content, the agglomerate reaches a state of saturation called the capillary state. In this state, the strength of the agglomerates is due to the capillary pressure. In the funicular state, both pendular bridges and capillary pressure provide strength to the agglomerates. The different saturation states in agglomerates are shown in Figure 1.4.

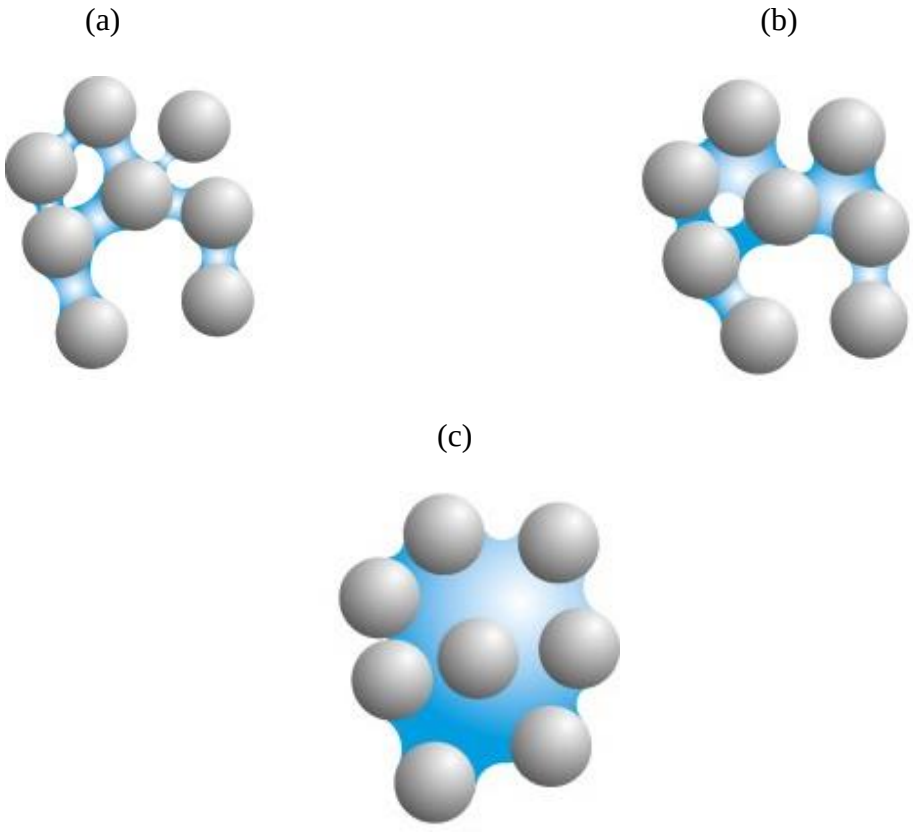

Figure 1.4: Different saturation states of binder in agglomerates. (a) Pendular State, (b) Funicular State, and (c) Capillary State. (Washino et al. (18))

The strength of the agglomerate depends on the liquid amount (strength of each liquid bridge) and the number of bridges that hold the grains together. The coordination number is the number of liquid bonds that a particle shares with its neighbors, and its value depends on the solid fraction, which defines how close the agglomerate is packed.

1.3.3 Hydrodynamic Modeling and Computational Methods

In order to analyze the effects of the hydrodynamics and properties of the reactor materials on the overall capacity and efficiency of the reactor, detailed modeling of the reactor based on physics is needed. Anderson (6) and Gidaspow (19) were the pioneers in introducing the idea of using computational fluid dynamics (CFD) to model the hydrodynamics of granular material in fluidized beds. Following their work, many CFD models have been developed in the last few decades, contributing towards a better understanding of fluidized beds. With the development of faster computers and more efficient numerical methods, CFD modeling has become an integral tool for a better understanding of the complicated interaction between phases in a fluidized bed.

Sinclair (20) characterized the hydrodynamics of gas-particle flows in two different classifications of frameworks to develop the models, namely the Eulerian and Lagrangian frameworks. In the Eulerian approach, the particle (or solid) phase is assumed to be a continuous medium, and the interaction between the phases is modeled using a separate set of equations. In contrast to the Eulerian model, in the case of Lagrangian modeling, the governing equations of motions are solved separately for each individual particle in the field. As one expects, for Lagrangian modeling, the high number of particles to be tracked in order to evaluate the average flow property requires more time and more computing power. In the Eulerian framework, only

one equation of motion is solved for each phase, and hence it requires equations of closure to describe the phases as a continuum. Eulerian models can be used to simulate systems of practical importance with comparatively fewer computational demands.

There can also be a multiscale modeling of gas-particle systems where the system is solved in different scales and then specific parameters are used to couple the different scales. Multiscale models are described in Figure 1.5.

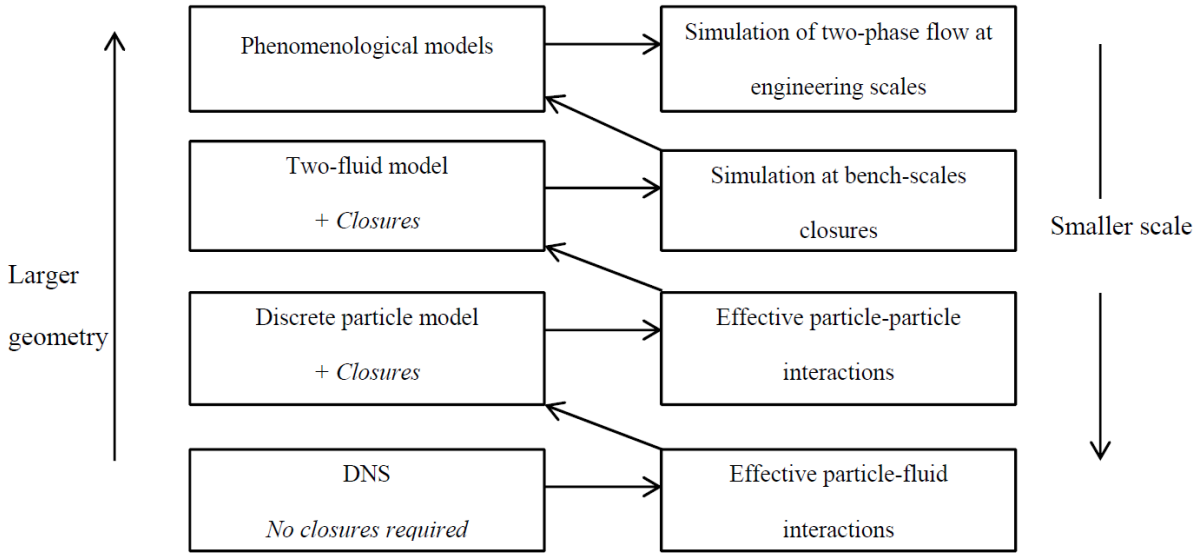

Figure 1.5: Multiscale modeling approach (Deen et al. (21))

While solving the system starting from lower scales and moving to upper scales, the most basic scale is solved using direct numerical simulation (DNS), which does not need any closure. A no-slip boundary condition is used at the interface between the particulate and gas phase. Moving up on the scale order, the Discrete Particle Model is used where the particle phase is solved using a Lagrangian framework and the fluid phase is solved using the Eulerian framework. At the higher

scales, two-fluid or multi-fluid models are considered where each phase is considered as an interacting continuum.

Computational simulations using these models are generally applied to laboratory-scale domains. To move and simulate an industrial-scale domain, a meaningful combination of different scale models must be used that preserve the physics but use less computational power. Generally, the lower scale model, which considers the interaction in the minute scale, is used to provide a closure to describe the interaction of coarse grains in the higher scales. The momentum distribution in a particle phase in multi-fluid models is averaged, and there are many ways to model it using partial differential equations (PDEs), depending on the problem statement. In early attempts to use CFD in fluidized beds, large enough regions were chosen to enclose many particles, but they were relatively smaller compared to the container (6, 19). In these regions, the equation of motion for the center of mass of the particles was averaged. A detailed theory on averaging the equations for a Eulerian approach to two-phase fluidized bed is discussed by Enwald et al. (22) and is beyond the scope of this thesis.

For a Eulerian two-phase model, there are two continuous phases, represented by two mass conservation (or continuity) equations, two momentum equations in each direction and two energy equations. Closure laws are further needed to close continuity, momentum and energy equations. A general method to develop a two-fluid model is described by Enwald et al. (22). A similar procedure could be used to extend the model to a multi-fluid model. These multi-fluid models are highly applicable to a wide range of practical problems and are still computationally less demanding than the Lagrangian model. Many computational models have been developed

and used to predict the behavior of fluidized beds (23). Esmaili et al. (24) calibrated the drag coefficient expression and conducted simulations to study its effects on the behavior of fluidized beds and reported that the drag model proposed by Gidaspow (25) is an appropriate model to use in fluidized beds.

1.3.4 Breakage of Agglomerates

Previous attempts have been made to model the breakage of agglomerates based on shear (26, 27) and the number of inter-particle contacts broken (28, 29). Moreno et al. (28) used a phenomenological approach to model the breakage in agglomerates based on the damage ratio, the ratio of the number of bonds broken to the initial number of bonds. He studied the properties of breakage for different surface energy values and reported that the agglomerates do not break unless the impact velocity reaches a minimum value. Feng et al. (30) used a population balance method to model the breakage, considering the effects of interior forces in the agglomerates and fluid shear. The expression for particle-size distribution, which defines the probability of an agglomerate to break into different sizes, was simplified, and only binary and ternary breakages were considered. In binary breakage, the agglomerates break into two halves, where in ternary breakage, the agglomerates were assumed to break into one half and two quarter-sized pieces. This model does not consider the other kinds of breakage where the agglomerates, in reality, could break into two unequal-sized pieces and with a large difference in sizes. Also, they used the global velocity gradient as the time scale for the breakage frequency, and that led to the need to introduce a large empirical coefficient.

Weber et al. (14) performed experiments to investigate the importance of abrasion of agglomerates. They used agglomerates made of coke and glass beads and studied the effect of different liquid binders and superficial gas velocities on the survival of agglomerates in a laboratory-scale fluidized bed. They reported that agglomerates abraded completely over time and concluded that the effect of abrasion is very important to the stability of agglomerates. They also reported that for higher liquid content in the glass beads and silica sand experiments, growth of agglomerates was dominant to a point, and then the agglomerates started to abrade. Shamlou et al. (31) studied the hydrodynamic effect on the particle breakage of granules made of glass beads and polymer. They found that for lower velocities, the breakage occurred mainly due to abrasion rather than fragmentation.

Although there are a number of studies that model fragmentation (28, 30), there is limited work on modeling the abrasion of agglomerates. Abrasion is a continuously occurring process inside fluidized beds and cannot be neglected. Hence, it is very important to develop a mechanistic model of abrasion that is based on the physics of the process and not dependent on empirical fitting parameters.

1.4 Objectives

The main objective of this thesis is to shed light on the complexities of breakage phenomenon and propose an approach to enhance modeling of agglomerate breakage. The objectives can be listed as follows,

- Develop a novel mechanistic, non-empirical model to determine the abrasion of agglomerates by defining the frequency of abrasion.

- Test the model for variation of a set of parameters, and compare with available experimental data.
- Evaluate the importance of abrasion in the breakage process.

1.5 Outline of Thesis

Chapter 2 presents the theory and model equations in a Eulerian framework needed to define the behavior of the fluid and solid phases, based on the kinetic theory of granular flow (KTGF).

Chapter 3 deals with the development of a novel model that describes the extent of abrasion in fluidized beds based on abrasion frequency. Abrasion frequency is derived using the collision rate between the granular phases. The success of abrasion due to particle collisions is expressed based on probability terms that are defined based on the coordination number, energy of collisions, and the geometry of agglomerates. Mass transfer rates between the phases and agglomerate diameter after abrasion are also defined.

Chapter 4 focuses on the comparison of results obtained from simulations in ANSYS Fluent and experimental data. A fragmentation approach is suggested which could be combined with an abrasion model in the future to obtain more realistic results for agglomerate breakage.

Chapter 5 presents the summary, conclusions and suggestions for further work

Chapter 2: Theory and Background

As discussed in the previous chapter, the modeling of gas-solid flow can generally be achieved using two different modeling approaches, namely Eulerian-Eulerian and Eulerian-Lagrangian models. Eulerian-Lagrangian models solve solid motion by tracking individual particles and need very high computational power that makes application of these models to the large-scale fluid coking process impractical. In this thesis, the granular phase is modeled by coupling the Eulerian-Eulerian approach and the kinetic theory of granular flows (KTGF).

2.1 Model Equations

The three-phase model using the Eulerian-Eulerian approach is used to simulate the flow of the granular materials in the fluidized bed. In the Eulerian-Eulerian approach, the granular phase is considered as a continuous medium, interacting with the other phases, and the number of granules in a control volume is determined using the volume fraction and particle diameter. The equations discussed in this thesis are based on an ensemble averaging approach. Hence, it is important to apply the necessary closure to the model to simulate the solid phase as a continuous medium. The properties like solid bulk viscosity, solid-gas momentum exchange, solid pressure and shear have to be calculated using physically meaningful models for a good understanding of the behavior of granular flows. As the phases are assumed to be continuous, the sum of the volume fractions of all phases equals to one. Hence, the equation for the volume fraction can be written (32) as,

$$\sum_{i=1}^{N} \varepsilon_i = 1 \qquad \textbf{(2.1)}$$

where N denotes the overall number of phases in the system and ε_i denotes the volume fraction of the phase i. The volume fraction of the solid phase or secondary phase, s, is generally called the solid fraction, and the volume fraction of the gaseous phase or primary phase, g, is called the void fraction. In the Eulerian-Eulerian model, multiple solid phases can also be considered and simulated, and the conservation equations are written for each phase separately.

2.1.1 Equations of Continuity

The general equation of continuity is the mass conservation of the fluid in a control volume. The rate of change of the mass of the fluid at any control volume can be expressed in terms of density (ρ_i) and volume fraction (ε_i) as,

$$\frac{\partial}{\partial t}(\varepsilon_i \, \rho_i)$$

Similarly the mass flow of the fluid can be expressed using the velocity field vector ($\overrightarrow{v_i}$) as, $\nabla(\, \varepsilon_i \, \rho_i \, \overrightarrow{v_i})$. Using the law of conservation of mass across the control volume, the sum of the rate of change in the mass and the mass flow should be equal to the amount of mass generated in the control volume, or simply the mass source S_i. In addition to these, there can also be mass transfer between the phases. Hence the equation of continuity can be written as follows (32),

$$\frac{\partial}{\partial t}(\varepsilon_i \, \rho_i) + \nabla . \, (\, \varepsilon_i \, \rho_i \, \overrightarrow{v_i}) = \sum_{j=1}^{N} (\dot{m}_{ij} - \dot{m}_{ij}) \, + S_i \qquad \textbf{(2.2)}$$

where the term $\dot{m}_{i,j}$ represents the mass transfer from the phase j to the phase i and is calculated based on the agglomeration or breakage happening in each phase. Hence the summation of all the individual mass transfer terms gives the overall transfer of mass from or into the phase i. For a fluidized bed reactor, the source term, S_i, is taken as zero. Hence the Equation (2.2) reduces to

$$\frac{\partial}{\partial t}(\varepsilon_i \rho_i) + \nabla . (\varepsilon_i \rho_i \overrightarrow{v_i}) = \sum_{j=1}^{N} (\dot{m}_{ij} - \dot{m}_{ij}) \quad \textbf{(2.3)}$$

2.1.2 Momentum Equations

2.1.2.1 Primary Phase Momentum Equations

The ensemble averaged momentum equation for the primary phase, g, can be written (32) as,

$$\frac{\partial}{\partial t}(\varepsilon_g \rho_g \overrightarrow{v_g}) + \nabla . (\varepsilon_g \rho_g \vec{v}_g \vec{v}_g) = -\varepsilon_g \nabla p + \nabla . \bar{\bar{\tau}}_g + \varepsilon_g \rho_g \vec{g} + \sum_{s=1}^{M} (\vec{R}_{sg} + \dot{m}_{sg}(\vec{v}_s - \vec{v}_g) - \dot{m}_{gs}(\vec{v}_g - \vec{v}_s) + \vec{F}_g + \vec{F}_{lift,g} + \vec{F}_{vm,g} \quad \textbf{(2.4)}$$

where M denotes the number of secondary phases. The first and second terms on the left-hand side of the equation represent the unsteady acceleration and convective acceleration of the flow, respectively. The first two terms on the right-hand side of the equation represent the change in pressure and shear stress tensor, respectively. The stress tensor term can be written as,

$$\bar{\bar{\tau}}_g = \varepsilon_g \mu_g (\nabla \vec{v}_g + \nabla \vec{v}_g^T) + \varepsilon_g \left(\lambda_g - \frac{2}{3}\mu_g\right) \nabla . \vec{v}_g \bar{\bar{I}} \quad \textbf{(2.5)}$$

where μ_g and λ_g denote the shear viscosity and bulk viscosity, respectively. The term $\nabla \vec{v}_g^T$ denotes the transpose of the velocity gradient and $\bar{\bar{I}}$ denotes the identity matrix.

While the third term of the equation (2.4) denotes the force of gravity, the next group of terms denote the interaction between the gaseous phase, g, and the secondary phase, s. In this group, $\vec{R}_{sg}$ denotes the force of interaction between the phases (also called drag force), and the rest of

the terms denote the change in momentum due to mass transfer between the phases. And the last set of terms, $\vec{F}_g$, $\vec{F}_{lift,g}$ and $\vec{F}_{vm,g}$, denote the external force, lift force and the force of virtual mass, respectively. As the drag or interaction force arises due to the exchange of momentum between the phases, $\vec{R}_{sg}$ can be written (32) as,

$$\sum_{s=1}^{M} \vec{R}_{sg} = \sum_{s=1}^{M} K_{sg} \left(\vec{v}_s - \vec{v}_g\right) \tag{2.6}$$

as a product of the coefficient of exchange of momentum between phases, K_{sg}, and their relative velocity (also called slip velocity).

2.1.2.2 Secondary/Solid Phase Momentum Equations

The ensemble average momentum equation for a solid phase s can be written as (32),

$$\frac{\partial}{\partial t}(\varepsilon_s \rho_s \overrightarrow{v_s}) + \nabla . (\varepsilon_s \rho_s \vec{v}_s \vec{v}_s)$$

$$= -\varepsilon_s \nabla p - \nabla p_s + \nabla . \bar{\bar{\tau}}_s + \varepsilon_s \rho_s \vec{g} + \sum_{q=1}^{M} (\vec{R}_{qs} + \dot{m}_{qs}(\vec{v}_q - \vec{v}_s) \tag{2.7}$$

$$- \dot{m}_{sq}(\vec{v}_s - \vec{v}_q)) \quad + \vec{F}_g + \vec{F}_{lift,s} + \vec{F}_{vm,s}$$

where p_s denotes the solid pressure, $\vec{R}_{qs}$ denotes the interaction force between the solid phase s and the gaseous or one of the other solid phases q, and M is the number of phases other than s. The rest of the terms are similar to terms in equation (2.4). The interaction force term, $\vec{R}_{qs}$, can be expressed by,

$$\sum_{q=1}^{M} \vec{R}_{qs} = \sum_{q=1}^{M} K_{qs} \left(\vec{v}_q - \vec{v}_s\right) \tag{2.8}$$

as a product of the coefficient of exchange of momentum between phases, K_{qs}, and their relative velocity (also called slip velocity) where $K_{qs} = K_{sq}$. The force of the interaction in the solids can be due to either the drag induced by the gas flowing around it or the collision of particles between the phases s and p.

2.1.3 Gas-Solid Interaction

The interaction between the gas and the solid phases arises due to the flow of the gas around the solid particles, which results in the exchange of momentum between the phases. This exchange of momentum is what drives the fluidized bed by lifting the solid particles against gravity. The gas-solid coefficient of momentum exchange, K_{sg}, can be expressed as

$$K_{sg} = \frac{\varepsilon_s \, \rho_s \, f}{\tau_s} \tag{2.9}$$

where f depends on the exchange-coefficient model chosen, and τ_s denotes the relaxation time of the solid phase and is expressed as

$$\tau_s = \frac{\rho_s \, d_s^2}{18 \, \mu_g} \tag{2.10}$$

where d_s denotes the diameter of the solid particles in the phase s. The coefficient of momentum exchange is a function of coefficient of drag, C_D and Reynolds number, Re_s. The drag model proposed by Gidaspow (25) is an appropriate model to use in fluidized beds. The model is a combination of the drag models proposed by Wen and Yu (33) and the equation proposed by Ergun (34) with the transition occurring at a void-fraction of value 0.8. Using the appropriate expression for f, the Gidaspow model can be written {Gidaspow, 1991 #47} as,

$$K_{sg} = \begin{cases} \frac{3}{4} C_D \left(\frac{\varepsilon_s \, \varepsilon_g \rho_g \left| \vec{v}_g - \vec{v}_s \right|}{d_s} \right) \varepsilon_g^{-2.65} & , \quad \varepsilon_g > 0.8 \\ 150 \left(\frac{\varepsilon_s (1 - \varepsilon_g) \mu_g}{\varepsilon_g \, d_s^2} \right) + 1.75 \left(\frac{\rho_g \, \varepsilon_s \left| \vec{v}_g - \vec{v}_s \right|}{d_s} \right), & \quad \varepsilon_g \leq 0.8 \end{cases} \tag{2.11}$$

where the coefficient of drag is the same as in the Wen and Yu (33) model and is expressed as

$$C_D = \frac{24}{\varepsilon_g Re_s} \left[1 + 0.15 \left(\varepsilon_g Re_s \right)^{0.687} \right] \tag{2.12}$$

where Re_s is the Reynolds number of the particulate phase and can be written as

$$Re_s = \frac{\rho_g \, d_s \left| \vec{v}_g - \vec{v}_s \right|}{\mu_g} \tag{2.13}$$

2.2 Kinetic Theory of Granular Flows

Fluid flows are typically associated with a no-slip boundary condition. But in a granular medium, the fluid moves with respect to the solid boundaries, and the behavior of the flow highly depends on the boundary conditions provided. As the solid phases are considered to be a continuum in the Eulerian-Eulerian approach, an analogy between the granular phase and the kinetic theory of dense gases is built using the kinetic theory of granular flows (KTGF). A detailed understanding of the KTGF derivation can be found here (19, 35-37); only the main ideas of KTGF are discussed in this thesis. Most of the equations in this chapter are presented for a system with a single solid phase, and extending them to multiple solids phases can be done. Such extensions that are within the scope of this thesis are discussed in the following chapters. As KTGF is a semi-empirical model, there are many empirical expressions available in the literature. Only the expressions used most commonly for a fluidized bed system are discussed here.

2.2.1 Granular Temperature

The granular temperature, θ_s, of a phase describes the energy associated with the random fluctuation of the solid particles due to collision and translation. The fluctuation energy associated with the granular phase, E_{θ_s}, can be expressed as (38)

$$E_{\theta_s} = \frac{3}{2}\,\theta_s = \frac{1}{2}\langle \vec{C}_s . \vec{C}_s \rangle \tag{2.14}$$

$$\theta_s = \frac{1}{3}\langle |\vec{C}_s^2| \rangle \tag{2.15}$$

where $\vec{C}_s$ denotes the random fluctuation component of the granular velocity, $\vec{c}_s$, of the phase s and can be written as

$$\vec{c}_s = \vec{U}_s + \vec{C}_s \tag{2.16}$$

where $\vec{U}_s$ denotes the mean velocity of the granular phase and $\langle \quad \rangle$ is used to describe the ensemble averaging of the fluctuating component of velocity. For a system with multiple solid phases, the two-phase kinetic theory can be extended to multiple phases. Goldschmidt (39) derived the usage of the kinetic theory of granular flows (KTGF) for a multi-phase system. The transport equation for the granular temperature can be derived using Gidaspow (19) as

$$\frac{3}{2}\left[\frac{\partial}{\partial t}(\varepsilon_s \rho_s \theta_s) + \nabla.(\varepsilon_s \rho_s \vec{v}_s \theta_s)\right] = \left(-p_s \bar{\bar{I}} + \bar{\bar{\tau}}_s\right) : \nabla \vec{v}_s + \nabla.\left(k_{\theta_s} \nabla \theta_s\right) - \gamma_{\theta_s} + \varphi_{ps} \tag{2.17}$$

which describes the transformation of the mechanical energy of the granular flow into the random motion of the granules, which is later dissipated into internal energy. This equation can also be interpreted as the conservation of fluctuation energy. In equation (2.17), $\left(-p_s \bar{\bar{I}} + \bar{\bar{\tau}}_s\right) : \nabla \vec{v}_s$ denotes the contribution of surface forces (solid stress tensor) to the generation of energy, and $\nabla.\left(k_{\theta_s} \nabla \theta_s\right)$ denotes the diffusion of energy where k_{θ_s} represents the diffusion coefficient which was defined by Syamlal et al. (32) as

$$k_{\theta_s} = \frac{15\ \varepsilon_s \rho_s d_s \sqrt{\theta_s\ \pi}}{4\ (41 - 33\eta)} \left[1 + \frac{12}{5}\eta^2(4\eta - 3)\varepsilon_s g_{0,ss} + \frac{16}{15\pi}\ (41 - 33\eta)\eta\varepsilon_s g_{0,ss} \right] \quad \textbf{(2.18)}$$

where $g_{0,ss}$ denotes the radial distribution function and is discussed in the next sub-section 2.2.3 and η is defined as

$$\eta = \frac{1}{2}\ (1 + e) \quad \textbf{(2.19)}$$

where e is the coefficient of the restitution of the collision of particles. In Equation (2.17), the exchange of energy between the solid phase s and the other interacting phase p (solid or fluid) is denoted by φ_{ps} and expressed as (19)

$$\varphi_{ps} = -3K_{ps}\theta_s \quad \textbf{(2.20)}$$

and the dissipation of energy due to the collisions of particles is denoted by γ_{θ_s} and is expressed (40) as

$$\gamma_{\theta_s} = \frac{12\ (1 + \ e^2) g_{0,ss}}{d_s\sqrt{\pi}}\ \varepsilon_s^2 \rho_s \theta_s^{3/2} \quad \textbf{(2.21)}$$

2.2.2 Solids Pressure

Granular flows are compressible when the solid fraction of the phases is lower than the maximum threshold value, $\varepsilon_{s,max}$. As the maximum possible solid fraction of random close packing for uniform spheres is 0.63, this value is generally chosen as the maximum threshold in granular flows. In the compressible regime, solid pressure, which appears in Equation (2.7), is generated in the flow and can be expressed (40) as

$$p_s = \ \varepsilon_s \rho_s \theta_s + \ 2\rho_s\ (1 + e)\ \varepsilon_s^2 g_{0,ss} \theta_s \quad \textbf{(2.22)}$$

where θ_s denotes the granular temperature, e denotes the coefficient of restitution of the collision of particles, and $g_{0,ss}$ denotes the radial distribution function and is discussed in the next sub-section.

2.2.3 Radial Distribution Function

The radial distribution function $g_{0,ss}$ in Equation (2.22) is a factor that adjusts the number of collisions occurring between the particles when the solid fraction reaches the maximum threshold value, $\varepsilon_{s,max}$. This function can also be understood as the non-dimensional distance between the spheres.

The radial distribution function controls the transition of the flow between the compressible and incompressible regimes. When the volume fraction of the solid phase reaches the maximum, the compressible flow becomes incompressible. The radial distribution function is defined as a function of the solid fraction, and there are many expressions available depending on the flow properties. For one-phase systems, the radial distribution function can be expressed as suggested by Ogawa (41) as

$$g_{0,ss} = \left[1 - \left(\frac{\varepsilon_s}{\varepsilon_{s,max}}\right)^{\frac{1}{3}}\right]^{-1} \quad \textbf{(2.23)}$$

where $\varepsilon_{s,max}$ = 0.63 and the radial distribution function of a granular phase can be extended to multiphase systems (32) as

$$g_{0,ss} = \left[1 - \left(\frac{\varepsilon_s}{\varepsilon_{s,max}}\right)^{\frac{1}{3}}\right]^{-1} + \frac{1}{2}\, d_s \sum_{k=1}^{N} \frac{\varepsilon_k}{d_k} \quad \textbf{(2.24)}$$

2.2.4 Solid Shear Stress

The solid shear stress tensor, $\bar{\bar{\tau}}_s$, in Equation (2.7) can be understood as the combination of frictional, collisional, and kinetic tensors. In flows with a low volume fraction (dilute flows), the translation and random fluctuation of the granular particles contribute to the kinetic part of stress and dissipation. In flows with a higher volume fraction (concentrated flows), the number of collisions between the particles of the phases becomes considerable, and there is energy dissipation and stress. When the concentration of granular phases becomes large (generally 50% of the volume fraction or more), there is frictional sliding between the particles, which results in the frictional component of dissipation and stress. Kinetic, collisional, and frictional forms of stresses in the granular flow are described in Figure 2.1. The frictional stress tensor is defined as a function of the volume fraction of the granular phase, and it becomes very large when the volume fraction reaches the threshold value, $\varepsilon_{s,max}$.

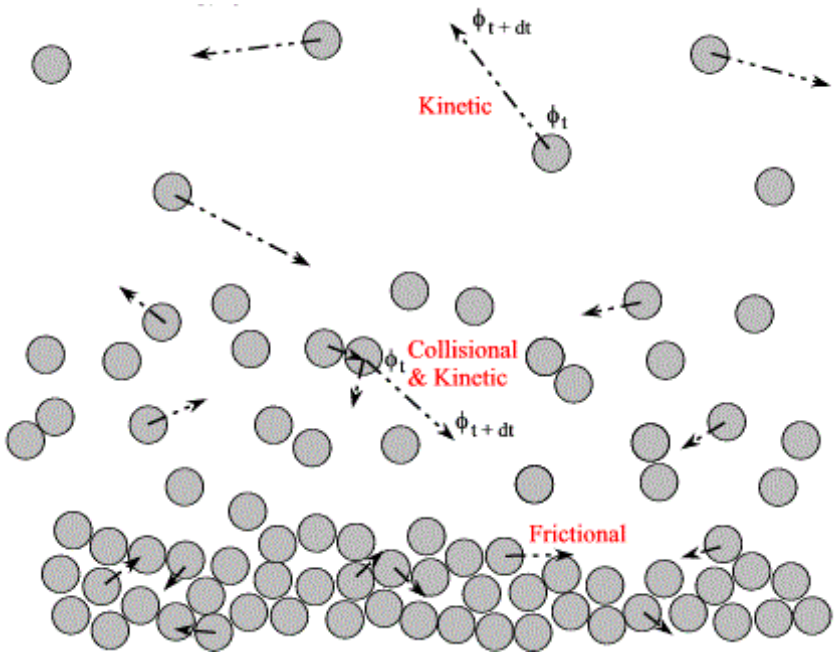

Figure 2.1: Different types of energy dissipation in granular flows (Dartevelle (42))

Syamlal and O'Brien (28) proposed to consider the granular phase as incompressible when the volume fraction approaches the threshold maximum. This avoids the problem of defining a frictional stress tensor that could be replaced by the solid pressure. In this formulation, the solid pressure is calculated to avoid the volume fraction becoming more than the threshold, and it becomes zero when the volume fraction is less than $\varepsilon_{s,max}$. Using this approach, the flow of the granular medium can be divided into two regimes—viscous and plastic. In viscous regimes, the stress is caused due to the collisional and translational transfer of momentum. It is also called a rapidly shearing regime. In a plastic regime, the stress is caused by the Coulomb friction that arises during the contact between the granular particles. It is also called a slowing shearing regime, but does not generally occur in fluidized beds.

Hence the solid shear tensor from Equation (2.7) is written as

$$\bar{\bar{\tau}}_s = \varepsilon_s \mu_s (\nabla \vec{v}_s + \nabla \vec{v}_s^T) + \varepsilon_s \left(\lambda_s - \frac{2}{3}\mu_s\right) \nabla . \vec{v}_s \, \bar{\bar{I}} \quad \textbf{(2.25)}$$

where μ_s and λ_s are the shear viscosity and bulk viscosity of the solid phase. As discussed earlier, the shear viscosity can be written as the summation of kinetic, collisional, and frictional viscosities as

$$\mu_s = \mu_{s,col} + \mu_{s,kin} + \mu_{s,fric} \quad \textbf{(2.26)}$$

The frictional viscosity is zero initially and starts to have a non-zero positive value if the maximum threshold volume fraction is reached. The individual components of viscosities can be written as (32, 40)

$$\mu_{s,col} = \frac{4}{5} \varepsilon_s \rho_s d_s g_{0,ss} (1+e) \left(\frac{\theta_s}{\pi}\right)^{0.5} \quad \textbf{(2.27)}$$

$$\mu_{s,kin} = \frac{10 \, \rho_s d_s \sqrt{\pi \, \theta_s}}{96 \, \varepsilon_s \, g_{0,ss}(1+e_{ss})} \left[1 + \frac{4}{5} \varepsilon_s g_{0,ss}(1+e)\right]^2 \quad \textbf{(2.28)}$$

$$\mu_{s,fric} = \frac{p_s \, \sin\varphi}{2\sqrt{I_{2D}}} \quad \textbf{(2.29)}$$

where p_s is the solid pressure expressed in Equation (2.22). The terms φ and I_{2D} are the angle of internal frication and the second invariant of the deviatoric stress tensor, respectively. The bulk viscosity can be written using the expression by Lun et al. (40) as

$$\lambda_s = \frac{4}{5} \varepsilon_s \rho_s d_s g_{0,ss} (1+e_{ss}) \left(\frac{\theta_s}{\pi}\right)^{0.5} \quad \textbf{(2.30)}$$

In this thesis, the kinetic theory equations for granular phases were solved using an in-built solver in ANSYS Fluent.

Chapter 3: Modeling of Abrasion

In this chapter, a new model for the modeling of erosion of agglomerates is proposed. It results in the development of a novel breakage kernel that defines the rate of abrasion of the agglomerates as a function of their interaction with the particulate phase. In fluidized beds, the interaction between the solid phases occurs as collisions between the different granular particles. As the granular phase is assumed to be a continuum, the interaction between the solid phases is defined as the momentum exchange, as in Equation (2.7). In this thesis, two solid phases are considered: a primary particle phase, denoted by p, and an agglomerate phase, denoted by a.

3.1 Frequency of Collisions

To define the interaction between the solid phases, the momentum exchange in continuum modeling is derived in terms of the collision between the phases. The rate of collision per unit volume between the granular particles of different phases depends on their relative approach velocity and number of particles and agglomerates. The collisions between the particles and the agglomerate are assumed to be inelastic. The area of the collisional plane between the particle and agglomerate, A_{pa}, also determines the rate of collision. The collisional plane is the circular plane joining the centers of the particle and the agglomerate. Hence, the number of collisions per second per unit volume can be then calculated as defined by Kolev (43) as

$$\dot{n}_{coll} = n_p n_a \, A_{pa} \left|\vec{v}_p - \vec{v}_a\right| \tag{3.1}$$

$$\dot{n}_{coll} = n_p n_a \frac{\pi}{4} \left(\frac{d_p + d_a}{2}\right)^2 \left|\vec{v}_p - \vec{v}_a\right| \tag{3.2}$$

where n_p and n_a represent the number of particles and agglomerates in a unit volume (number density), respectively. In Eulerian modeling, as the number density of the granular phases is expressed in terms of volume fraction, the number density can be rewritten as

$$n_p = \frac{\varepsilon_p}{\left(\frac{\pi {d_p}^3}{6}\right)} = \frac{6\,.\,\varepsilon_p}{\pi {d_p}^3} \tag{3.3}$$

where ε_p represents the solid fraction of the particle phase. Similarly, the number density of the agglomerate phase can be written as

$$n_a = \frac{6\,.\,\varepsilon_a}{\pi {d_a}^3} \tag{3.4}$$

As discussed in Section 1.3.4, the radial distribution function is a key parameter in determining the collision characteristics and needs to be introduced as a factor to correct the probability of collisions as a function of the volume occupied by the granules. Equation (2.24) describes the radial distribution function of a granular phase in a multiphase system. The overall radial distribution function between the particle and agglomerate phases, $g_{0,pa}$, can be expressed as derived by Gidaspow et al. (44) as

$$g_{0,pa} = \frac{d_p\, g_{0,aa} + d_a\, g_{0,pp}}{d_p + d_a} \tag{3.5}$$

Hence the collision frequency becomes

$$\dot{n}_{coll} = n_p n_a\, g_{0,pa}\ \frac{\pi}{4}\left(\frac{d_p + d_a}{2}\right)^2 \left|\vec{v}_p - \vec{v}_a\right| \tag{3.6}$$

$$\dot{n}_{coll} = n_p n_a\, \frac{d_p\, g_{0,aa} + d_a\, g_{0,pp}}{d_p + d_a}\ \ \frac{\pi}{4}\left(\frac{d_p + d_a}{2}\right)^2 \left|\vec{v}_p - \vec{v}_a\right| \tag{3.7}$$

3.2 Multi-phase Interaction

In this work, the assumption of no mass transfer between the gaseous and solid phases is made. Also the effects of the external, lift, and virtual mass forces are neglected. Hence, the equation (2.4), which represents the primary phase momentum balance as

$$\frac{\partial}{\partial t}\left(\varepsilon_g \rho_g \vec{v}_g\right) + \nabla . \left(\varepsilon_g \rho_g \vec{v}_g \vec{v}_g\right) = -\varepsilon_g \nabla p + \nabla . \bar{\bar{\tau}}_g + \varepsilon_g \rho_g \vec{g} + \sum_{s=1}^{M} (\vec{R}_{sg} + \dot{m}_{sg}\vec{v}_{sg} - \dot{m}_{gs}\vec{v}_{gs}) + \vec{F}_g + \vec{F}_{lift,g} + \vec{F}_{vm,g} \quad \textbf{(3.8)}$$

can be rewritten as

$$\frac{\partial}{\partial t}\left(\varepsilon_g \rho_g \vec{v}_g\right) + \nabla . \left(\varepsilon_g \rho_g \vec{v}_g \vec{v}_g\right) = -\varepsilon_g \nabla p + \nabla . \bar{\bar{\tau}}_g + \varepsilon_g \rho_g \vec{g} + \sum_{s=1}^{M} \vec{R}_{sg} \quad \textbf{(3.9)}$$

Unlike the gas phases, the mass transfer terms cannot be neglected for solid phases as there is transfer of mass between the solid phases due to abrasion of the agglomerate. The other terms denoting external, lift, and virtual mass forces can be neglected from the momentum balance equation of the granular phase,

$$\frac{\partial}{\partial t}(\varepsilon_s \rho_s \vec{v_s}) + \nabla . \left(\varepsilon_s \rho_s \vec{v}_s \vec{v}_s\right) = -\varepsilon_s \nabla p - \nabla p_s + \nabla . \bar{\bar{\tau}}_s + \varepsilon_s \rho_s \vec{g} + \sum_{q=1}^{M} (\vec{R}_{qs} + \dot{m}_{qs}\vec{v}_{qs} - \dot{m}_{sq}\vec{v}_{sq}) + \vec{F}_s + \vec{F}_{lift,s} + \vec{F}_{vm,s} \quad \textbf{(3.10)}$$

and hence the equation can be rewritten as

$$\frac{\partial}{\partial t}(\varepsilon_s \rho_s \overrightarrow{v_s}) + \nabla . (\varepsilon_s \rho_s \vec{v}_s \vec{v}_s)$$

$$= -\varepsilon_s \nabla p - \nabla p_s + \nabla . \bar{\bar{\tau}}_s + \varepsilon_s \rho_s \vec{g} + \sum_{q=1}^{M} (\vec{R}_{qs} + \dot{m}_{qs} \vec{v}_{qs} \quad \textbf{(3.11)}$$

$$- \dot{m}_{sq} \vec{v}_{sq})$$

3.2.1 Solid-Solid Interaction

In Equation (3.11), $\vec{R}_{qs}$ can be represented in terms of the momentum exchange coefficient as

$$\sum_{q=1}^{M} \vec{R}_{qs} = \sum_{q=1}^{M} K_{qs} (\vec{v}_q - \vec{v}_s) \quad \textbf{(3.12)}$$

where K_{qs} in the above equation represents the momentum exchange coefficients between the solid phases q and s. For the interaction between the agglomerate phase, a, and primary particle phase, p, the momentum exchange coefficient K_{pa} can be derived based on the collision frequency expression from Equation (3.7).

The overall drag force, $\vec{R}_{pa}$, exerted by the primary particles that are colliding with the agglomerates can be written in terms of the momentum exchange per collision, Δm, collision time, t_c, and collision frequency, $\dot{n}_{coll}$, (1, 45) as

$$\vec{R}_{pa} = \left(\frac{\Delta m}{t_c}\right) \dot{n}_{coll} \, t_c \quad \textbf{(3.13)}$$

$$\vec{R}_{pa} = \Delta m \, \dot{n}_{coll} \quad \textbf{(3.14)}$$

This can also be interpreted as the rate of momentum exchange per unit volume. Writing the momentum conservation equations for the collision between a primary particle and an agglomerate as

$$m_p \vec{v}_p' = m_p \vec{v}_p - \vec{J} \tag{3.15}$$

$$m_a \vec{v}_a' = m_a \vec{v}_a + \vec{J} \tag{3.16}$$

where $\vec{v}_p$ and $\vec{v}_p'$ are the velocities of primary particle before and after collision; $\vec{v}_a$ and $\vec{v}_a'$ are the velocities of the agglomerate before and after collision; the term $\vec{J}$ denotes the exchange in momentum from the particle phase to the agglomerate phase. For the coefficient of restitution, e, the initial and final approach velocities can be related as

$$\vec{v}_a' - \vec{v}_p' = -e\,(\vec{v}_a - \vec{v}_p) \tag{3.17}$$

Combining Equations (3.15), (3.16), and (3.17), the exchange of momentum, J, can be written as,

$$\vec{J} = \frac{-(1+e)\,(\vec{v}_a - \vec{v}_p)}{\left(\frac{1}{m_a} + \frac{1}{m_p}\right)} \tag{3.18}$$

Using $J = -\Delta m$, the drag force, $\vec{R}_{pa}$, can be rewritten as

$$\vec{R}_{pa} = \frac{(1+e)\,(\vec{v}_a - \vec{v}_p)}{\left(\frac{1}{m_a} + \frac{1}{m_p}\right)}\,\dot{n}_{coll} \tag{3.19}$$

From Equation (2.6), the drag force is written as $\vec{R}_{pa} = K_{pa}\,(\vec{v}_a - \vec{v}_p)$. Hence, using Equation (3.19), the momentum exchange coefficient can be written (45) as

$$K_{pa} = \frac{(1+e)}{\left(\frac{1}{m_a} + \frac{1}{m_p}\right)}\,\dot{n}_{coll} \tag{3.20}$$

$$K_{pa} = \frac{(1+e)}{\left(\frac{1}{m_a}+\frac{1}{m_p}\right)} n_p n_a \, g_{pa} \, \frac{\pi}{4}\left(\frac{d_p+d_a}{2}\right)^2 \left|\vec{v}_p - \vec{v}_a\right| \quad \textbf{(3.21)}$$

Replacing the number densities with their respective volumes and volume fractions and the masses with volumes and densities using Equation (3.4), Equation 3.21 can be simplified further to

$$K_{pa} = \frac{3\,(1+e)}{2\left(\rho_p\, d_p^3 + \rho_a\, d_a^3\right)} \rho_p \varepsilon_p \, \rho_a \varepsilon_a \left(d_p + d_a\right)^2 g_{pa} \left|\vec{v}_p - \vec{v}_a\right| \quad \textbf{(3.22)}$$

3.3 Pendular Bridge Properties

As discussed earlier, the strength of agglomerates depends on the total number of liquid bridges inside them and the strength of the individual bonds. The total number of bridges depends on the coordination number of the agglomerate. The coordination number, K_c, is defined as the number of bonds a single particle shares with its neighbors. The coordination number becomes higher as the interior packing of the agglomerates becomes denser. Based on experimental findings, Kusters (46) proposed a power law dependency of coordination number, K_c, over the solid fraction as

$$K_c = 15\varepsilon_s^{1.2} \quad \textbf{(3.23)}$$

where ε_s is the solid fraction of the agglomerate structure. The strength of the agglomerate also depends on the strength of the individual liquid bridges. Liquid bridge strength is governed by the liquid content, liquid properties, and particle-liquid contact angle. The liquid bridge volume, V_b, can be related to the overall liquid volume, V_l , as

$$V_b = V_l / N_b \quad \textbf{(3.24)}$$

where N_b represents the total number of liquid bridges in the agglomerate and can be related to the total number of granules in the agglomerate, and the coordination number as

$$N_b = \frac{N_p\, K_c}{2} \tag{3.25}$$

Equation (3.25) has the factor 1/2 since each bond is counted twice.

3.3.1 Rupture Energy of Pendular Bridges

The strength of the liquid bridges could be measured in terms of the energy required to break them. This thesis is based on the energy approach, and hence the energy required to break individual bonds is studied. Pitois et al. (47) derived an expression for the energy required to overcome the viscous forces to break the bond using a quasi-static approach. As shown in Figure 3.1, for a liquid bond formed between two particles of radius R, they calculated the bond breakage energy, E_b. The liquid bridge is held together through the viscous and capillary forces of the liquid, and hence the external force applied has to overcome both forces for a successful breakage. The bond breakage energy, E_b, can be taken as the summation of the energies needed to overcome the forces individually. Hence, the bond breakage energy can be written as

$$E_b = E_{visc} + E_{cap} \tag{3.26}$$

where $E_{visc}$and E_{cap} are the energies needed to overcome the viscous and capillary forces, respectively.

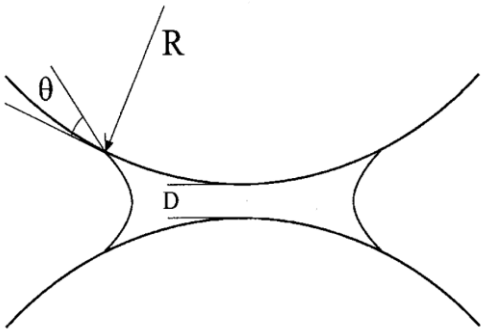

Figure 3.1 Liquid bridge between two spheres (Pitois et al. (47))

The capillary energy was calculated by Pitois et al. (47) by integrating the capillary force from a separation distance of zero to the distance at which the bond ruptures. The dimensionless rupture distance and the rupture distance were derived by Lian et al. (48) as

$$\widetilde{D}^{s}_{rupt} = \left(1 + \frac{\theta}{2}\right) \tilde{V}_b^{1/3} \tag{3.27}$$

$$D^{s}_{rupt} = \widetilde{D}^{s}_{rupt}.R_p = R_p.\left(1 + \frac{\theta}{2}\right) \tilde{V}_b^{1/3} \tag{3.28}$$

where θ is the contact angle between the liquid binder and the particle. The term $\tilde{V}_b$ denotes the dimensionless liquid bridge volume and was expressed as

$$\tilde{V}_b = \frac{V_b}{R_p^3} \tag{3.29}$$

where $R_p$is the radius of the primary particles. The dimensionless capillary energy, E_{cap}, then was derived by Pitois et al. (47) as

$$\tilde{E}_{cap} = 2\,\pi\, cos\theta \left\{\left(1 + \frac{\theta}{2}\right)(1 - A)\tilde{V}_b{}^{1/3} + \sqrt{\frac{2\,\tilde{V}_b}{\pi}}\right\} \tag{3.30}$$

where A is defined as

$$A = \left(1 + \frac{2\,\tilde{V}^{\frac{1}{3}}}{\pi\,(1+\frac{\theta}{2})^2}\right)^{1/2} \quad \textbf{(3.31)}$$

The capillary bond energy, E_{cap}, was defined in terms of the non-dimensional capillary energy, $\tilde{E}_{cap}$, as (47)

$$E_{cap} = \tilde{E}_{cap} \times \gamma\, R_p^2 \quad \textbf{(3.32)}$$

hence E_{cap} can be written as

$$E_{cap} = 2\,\pi\, cos\theta\ \gamma\, R_p^2 \left\{\left(1+\frac{\theta}{2}\right)(1-A)\tilde{V}_b{}^{1/3} + \sqrt{\frac{2\,\tilde{V}_b}{\pi}}\right\} \quad \textbf{(3.33)}$$

Similar to the capillary energy, the viscous energy is derived by integrating the viscous forces, but from the asperity height, D_m, to the rupture distance. The dimensionless viscous energy was then derived by Pitois et al. (47) as

$$\tilde{E}_{visc} = \frac{3}{2}\pi\, Ca \left(Ln\left(\frac{A\sqrt{\pi}}{(1+A)^2}\right) - f(\tilde{D}_m)\right) \quad \textbf{(3.34)}$$

where Ca is the capillary number and depends on the viscosity, surface tension, and the relative velocity between the spherical particles, V_r , and was defined (47) as

$$Ca = \frac{\mu}{\gamma}\left|\vec{V_r}\right| \quad \textbf{(3.35)}$$

The expression for V_r is discussed in the next sub-section. The viscous energy, E_{visc}, was related to the non-dimensional viscous energy, $\tilde{E}_{visc}$, (47) as

$$\tilde{E}_{visc} = \frac{E_{visc}}{\gamma R_p^2}$$

Hence, E_{visc} can be written as

$$E_{visc} = \frac{3}{2}\pi\,\mu\,|\vec{V}_r|R_p^2\left(Ln\left(\frac{A\sqrt{\pi}}{(1+A)^2}\right) - f(\widetilde{D}_m)\right) \quad \textbf{(3.36)}$$

where the term $f(\widetilde{D}_m)$ is written as

$$f(\widetilde{D}_m) = Ln(\widetilde{D}_m) - 2\,Ln\left((\widetilde{D}_m) + \sqrt{\widetilde{D}_m{}^2 + 2\frac{\tilde{V}_b}{\pi}}\right) + \frac{1}{2}\,Ln\left(\pi\,\widetilde{D}_m{}^2 + 2\tilde{V}_b\right) \quad \textbf{(3.37)}$$

$\widetilde{D}_m$ denotes the dimensionless asperity height and can be written as

$$\widetilde{D}_m = \frac{D_m}{R_p} \quad \textbf{(3.38)}$$

where D_m denotes the asperity height. Figure 3.2 represents the asperities on the surface of a particle.

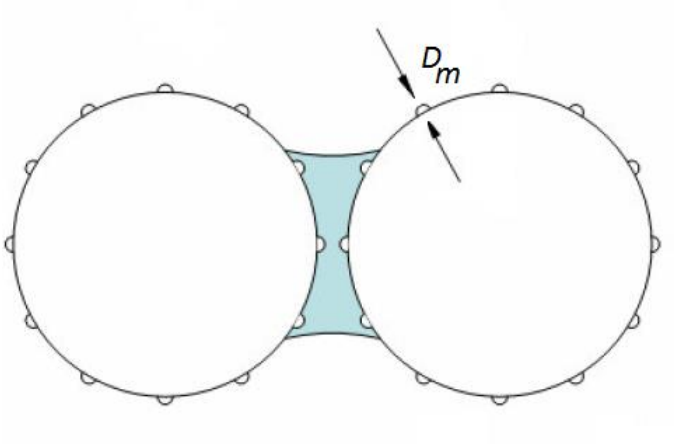

Figure 3.2: Asperities on the surface of particles, reproduced from Darabi et al. (49)

3.4 Collision Energy

The interaction between primary particles and agglomerates occurs through collisions of the first with the latter. As a result of the transfer of energy between particle and agglomerate, the liquid bridges in the agglomerate can break. The kinetic energy of the primary particle during collision with the agglomerate is written as,

$$E_c = \frac{1}{2}\, m_p \left(\vec{v}_p\right)^2 \tag{3.39}$$

where $\vec{v}_p$ is the velocity of the primary particle during collision. This kinetic energy is transmitted through the agglomerate causing a particle on the surface to vibrate. If this energy is greater than the bond energy, then breakage of one bond occurs. In Equation (3.36), to calculate viscous bond energy, the relative velocity between the particles $\vec{V}_r$ needs to be determined. The loss of kinetic energy is associated with the relative velocity of spheres as,

$$\frac{1}{2} m_p \left|\vec{V}_r\right|^2 = E_c \tag{3.40}$$

Hence, the relative velocity can be expressed as

$$\vec{V}_r = \vec{v}_p \tag{3.41}$$

3.5 Probability of Successful Abrasion

As multiple bonds need to be broken for a single particle to be abraded, the probability of successful abrasion depends on various factors like the energy of collision, coordination number, liquid bond strength, collisional site, etc. The various factors are discussed in the following section.

3.5.1 Probability of Breakage of a Bond

Most of the literature treats agglomeration as a result of collision and breakage caused by shear. Rajniak (53) defined the geometrical probability of agglomeration based on an accessible binder fraction, which is the probability of having a binder at the point of impact. During the collision of a particle at the binder site, agglomeration can be unsuccessful if the rebound velocity is high enough to break the bridge during its rebound. Rajniak (53) also proposed a condition that the collisional velocity needs to be less than a threshold for successful agglomeration (to prevent escape during rebound), which was defined in terms of a Stokes number. Moreno et al. (28), in their DEM simulations, reported that breakage of agglomerates did not occur unless a minimum impact velocity was reached. This is because below this velocity, the energy is not sufficient to break even a single bond.

Shamlou et al. (54) used an exponential function to define the probability as a function of agglomerate strength and shear. When agglomerate strength reaches infinity, the probability is zero, and when the agglomerate strength is zero, the probability is one. That means weaker agglomerates definitely break, whereas stronger agglomerates resist breakage. The probability function was defined (54) as

$$P_{shear} = e^{-\frac{\sigma}{\tau}} \tag{3.42}$$

where σ and τ represent the agglomerate strength and shear stress, respectively. Similar exponential functions for probability have been used in the literature to describe the breakage probability. Pougatch et al. (55) used a similar expression to describe particle attrition in fluid cokers.

In the derivation of KTGF equations, the granules are considered as point objects and all collisions are assumed to be head-on collisions. But in reality, the particles collide with the agglomerates at different angles in a random fashion. Only the component of mean velocity that is aligned with the liquid bridge in the agglomerates is responsible for the breakage**.** An exponential distribution is assumed for energy. When the collision energy reaches a very high value, bond breakage should occur (probability of breakage of one), and when the bond energy becomes high, no breakage should occur (probability of breakage of zero). To satisfy this condition, an exponential probability expression is proposed based on the energy of collision (E_c) and the bond energy (E_b) as

$$P_{bond} = e^{-\frac{E_b}{E_c}} \tag{3.43}$$

If the energy of collision is greater than the bond breaking energy, E_b, then bond breakage occurs, and hence the probability of breakage is taken as P_{bond}. For collision energy less than E_b, the probability of bond breakage can be taken as zero.

3.5.2 Geometric Probability

The particle at the surface of an agglomerate is bonded with $K_c/2$ other particles through liquid bridges. In order for a particle to be abraded from the agglomerate, all of its bonds with the neighboring particles should be broken simultaneously. Figure 3.3 shows a particle at the surface of the agglomerate (shaded) bonded with four other particles. The active collision region is defined as the region at which simultaneous collisions need to occur for the successful abrasion of the shaded particle. For a particle of diameter d, (shaded in gray), the active collision region is the area shown in Figure 3.3.

$K_c/2$ successive collisions have to occur, in the region enclosed by the circle of diameter $3d$, for the particle at the center to be abraded, i.e., released. Hence, the geometric probability of a successful abrasion gives the probability of successive breakage of bonds occurring at the same particle site and is defined as the ratio of the number of collisions occurring at the active collision region to the total number of collisions, at a particular time step. Hence, the geometrical probability of a successful abrasion can be written as the ratio of the area of active collision region to the total cross-sectional area of the agglomerate. Hence, the geometric probability, P_{geom}, is proposed as

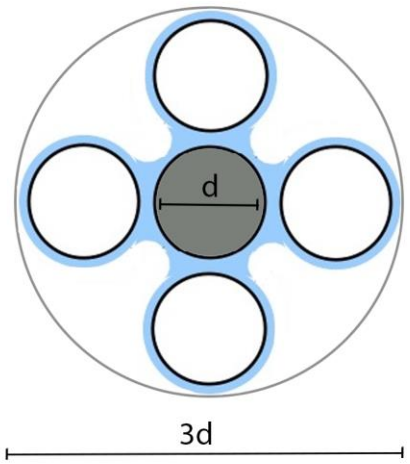

Figure 3.3: Active collision region for the shaded particle

$$P_{geom} = \frac{Area\ of\ active\ collision\ region}{Cross\ section\ area\ of\ agglomerate}$$

$$P_{geom} = \frac{\pi \frac{(3d_p)^2}{4}}{\pi \frac{(d)^2}{4}} = \frac{9\,{d_p}^2}{{d_a}^2} \tag{3.44}$$

3.5.3 Coordination Probability

The coordination probability, P_{co}, defines the number of bonds that need to be broken for the removal of a single particle. It is a constant value and is the inverse of half the coordination number K_c. Hence, the coordination probability is written as

$$P_{co} = \frac{1}{\left(\frac{K_c}{2}\right)} = \frac{2}{K_c} \tag{3.45}$$

3.5.4 Probability of Abrasion

The probability of breakage defines the overall probability of abrading a particle. It is a combination of the bond breakage probability, coordination probability, and geometric probability. Hence, the overall probability is written as

$$P_{br} = P_{bond}.P_{co}.P_{geom}$$

$$P_{br} = e^{-\frac{E_b}{E_c}} \left(\frac{2}{K_c}\right) \frac{9\,{d_p}^2}{{d_a}^2} \tag{3.46}$$

3.5.5 Energy Ratio

Energy ratio is defined as the ratio of collision energy (E_c) to the bond energy (E_b) and it denotes the total number of bonds that are broken per collision. The energy ratio is defined as,

$$E_r = \left(\frac{E_c}{E_b}\right) \tag{3.47}$$

3.5.6 Rate of Abrasion

Abrasion frequency is defined as the rate of abrasion of the particles from the surface of the agglomerate. It is the product of collision frequency, energy ratio and the abrasion probability. Hence, the frequency of abrasion (or abrasion rate) per unit volume can be written as,

$$\dot{n}_{ab} = \dot{n}_{coll}\, E_r P_{br} = n_p n_a\, g_{0,pa}\ \frac{\pi}{4}\left(\frac{d_p + d_a}{2}\right)^2 \left|\vec{v}_p - \vec{v}_a\right| e^{-\frac{E_b}{E_c}} \left(\frac{2}{K_c}\right)\left(\frac{E_c}{E_b}\right)\ \frac{9\, d_p}{{d_a}^2} \qquad \textbf{(3.48)}$$

In the above expression, the product of coordination probability and energy ratio gives the number of particles abraded per collision.

3.6 Mass Transfer Rate between Solid Phases

The rate of mass transfer between the phases per unit volume depends on the abrasion frequency, volume and density of the particles as

$$\dot{M}_{a,p} = \dot{n}_{ab}\, V_p\, \rho_p \qquad \textbf{(3.49)}$$

$$\dot{M}_{a,p} = n_p n_a\, g_{pa}\ \frac{\pi}{4}\left(\frac{d_p + d_a}{2}\right)^2 \left|\vec{v}_p - \vec{v}_a\right| e^{-\frac{E_b}{E_c}} \left(\frac{2}{K_c}\right)\left(\frac{E_c}{E_b}\right)\ \frac{9\, {d_p}^2}{{d_a}^2}\, V_p\, \rho_p \qquad \textbf{(3.50)}$$

where $\dot{M}_{a,p}$ is the rate of mass transfer from the agglomerate phase to the particulate phase per unit volume, and V_p and ρ_p are the volume and density of the primary particle, respectively.

3.7 Agglomerate Diameter after Abrasion

The abrasion frequency per agglomerate is the ratio of the abrasion frequency per unit volume to the number of agglomerates per unit volume. It can be written as

$$\dot{n}_{ab,a} = \frac{\dot{n}_{ab}}{n_a} \qquad \textbf{(3.51)}$$

Writing the agglomerate density in terms of volume fraction and volume of agglomerate, the abrasion frequency per agglomerate can be written as

$$\dot{n}_{ab,a} = \frac{\dot{n}_{ab}}{\varepsilon_a} V_a \tag{3.52}$$

Hence the volume of the agglomerate after a time step, Δt, is updated as

$$V_a' = V_a - \left(\dot{n}_{ab,a}\ V_p\right).\ \Delta t \tag{3.53}$$

Where V_{agg} and V'_{agg} are the volume of the agglomerate before and after the time step, Δt. Hence the diameter of the agglomerate is updated at the end of each time step as

$$d_a' = \left(\frac{6\ .\ V_a'}{\pi}\right)^{\frac{1}{3}} \tag{3.54}$$

Chapter 4: Results and Discussion

Simulations were performed based on the experimental work carried out by Dr. Sarah Weber at the Department of Chemical and Biochemical Engineering at the University of Western Ontario, Canada (14, 56). In the experiment, a constant mass of solid particles was added to a pre-determined liquid content and mixed thoroughly. The agglomerates were cylindrical and fabricated using a syringe-piston system, and by using different molds, agglomerates of different dimensions were produced. The main goal of these experiments was to study the stability, growth, and breakage of agglomerates in a lab-scale fluidized bed. Agglomerates were made using different sized particles and different liquid binders. The effects of physical parameters like the superficial gas velocity, agglomerate size, liquid binder content, and viscosity of the liquid binder on the stability were studied. Biodiesel liquids which, at room temperature, had similar physical properties to bitumen were used. The static bed height was approximately 0.15 m. Compressed gas was blown until the minimum fluidization was achieved and the fabricated agglomerate was then dropped from the top. Then the second fluidization line was opened and the velocity was controlled to achieve the desired superficial gas velocities. Figure 4.1 shows the schematic representation of the fluidized bed experiment.

In one of the experimental setups (14), the bed contents and the binder were chosen to have similar properties to bitumen in the industrial fluid coke process. The primary particles were coke particles of a Sauter diameter of $140\ \mu m$, as shown in Figure 4.2 (a). In the other experiment (56), the agglomerates were made of glass beads or silica sand, the binder was water, and the particle sizes were $171\ \mu m$, $282\ \mu m$, and $203\ \mu m$. The microscopic image is shown in Figure 4.2 (b). The parameters of the experimental setup are listed in Table 4.1.

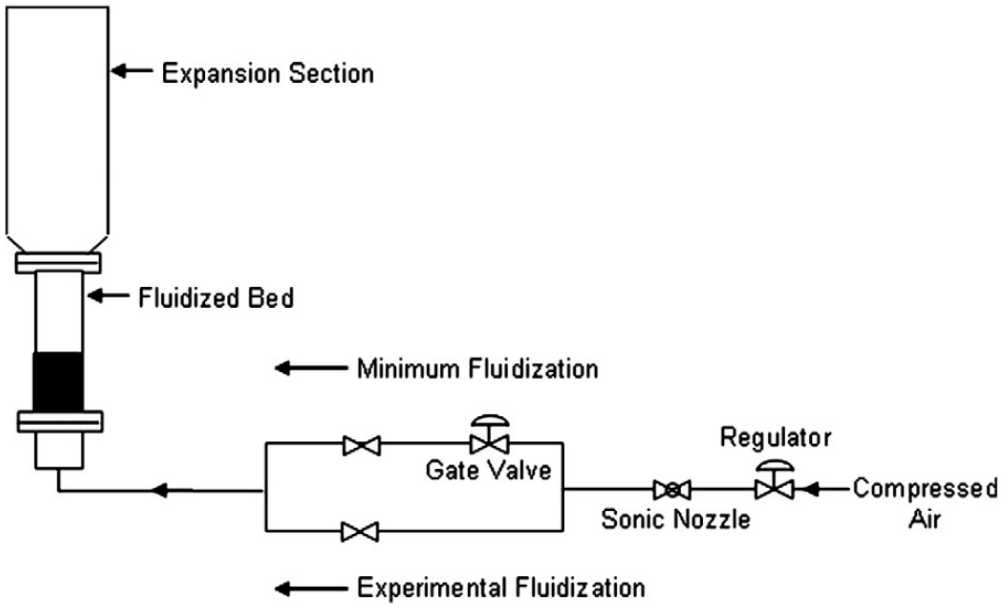

Figure 4.1: Schematic representation of fluidized bed experiment (Weber et al. (14))

Table 4.1: Fluidized bed parameters in lab-scale experiments (57)

Properties	Coke Binder Set up	Glass Beads, Silica sand Setup
Inlet Velocity	0.10, 0.17, 0.25, 0.34 m/s	0.18 m/s
Particle Diameter	140 μm	171 μm, 203 μm , 282 μm
Particle Density	1500 kg/m^3	2500 kg/m^3
Agglomerate Size (Diameter, Height)	0.0067 m, 0.0070m	0.0169 m, 0.0169 m
Agglomerate Density	1060 kg/m^3	1500 kg/m^3
Binder Viscosity	6.44, 9.79, 16.10, 64.7 10^{-3}N.s/m^2	0.000894 N.s/m^2
Binder Surface Tension	0.03 N/m	0.07 N/m
Liquid Contact Angle	0°	0°, 65°

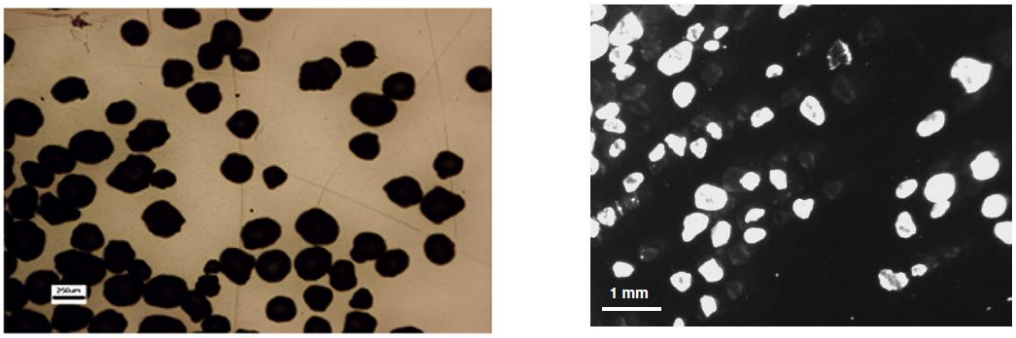

(a) (b)

Figure 4.2: Microscopic images of (a) coke and (b) silica sand particles used in experiments, reproduced from Weber (14, 56)

All the simulations were performed using ANSYS FLUENT 16 using a 2 Dimensional Double Precision (2ddp) Eulerian-Eulerian model. The boundary conditions and procedures were taken from these experiments where a lab-scale fluidized bed was set up with coke particles and glass beads as the bed material. A velocity inlet condition was assigned to the inlet boundary. No-slip and pressure outlet boundary conditions were used at the wall and outlet, respectively. A computational mesh consisting of 5544 elements was selected, and mesh independency was observed as solution was invariant with finer meshes. Convergence criteria of 10^{-3} for continuity and momentum equations and 10^{-4} for granular temperature were used for error monitoring. Second-order upwind discretization schemes were applied for the convection terms, and a time step of 10^{-4} s was found to be suitable to reach convergence, while being small enough to ensure negligible numerical errors. All the simulations took about two weeks on an Intel Xeon 2.66 GHz workstation. Plots of time-averaged void fraction and vertical component

of particle velocity were analyzed at different heights along the fluidized bed, to check for mesh independency.

4.1 Model Assumptions

The important assumptions of the model are listed below:

1. The agglomerates are assumed to be spherical and have the same volume to area ratio as the experiment.
2. The primary particles are assumed to be spherical and monodispersed.
3. All phases are assumed to be interpenetrating (Eulerian-Eulerian assumption).
4. All liquid content is present only in the liquid bridges.
5. Agglomerates have a uniform internal structure (constant coordination number); the internal volume fraction of the agglomerate in the experiments is reported as 0.59 and using Equation (3.23) by Kusters (46), the coordination number is calculated to be 7.96, which is approximated to 8 in this thesis.
6. For the purposes of the granular kinetic theory model, all the collisions are assumed to be dry and have a constant coefficient of restitution (e = 0.90); Darabi (51, 59) and Benyahia (52) reported that they had better predictions for fluidized beds for a coefficient of restitution value of 0.90, and the same value is set for all the collisions presented in this thesis. (A summary of the value of parameters is listed in the Table 4.2)

Table 4.2: Value of parameters in fluidized bed simulations

Coordination Number (K_c)	8
Coefficient of Restitution (e)	0.90
Liquid Content (mass)	1%

Packing Limit ($\varepsilon_{s,max}$)	0.63

4.2 Coke Binder Set up

Similar to the experiments, the dimension of the vessel domain is taken as 0.15 m x 1 m and is initially patched with primary particles to a height of 0.15 m, as shown in Figure 4.3 (a). The diameter of spherical agglomerate is chosen such that the volume to area ratio is consistent with the cylindrical agglomerate in the experiment. The initial volume patching of agglomerate is shown in Figure 4.3 (b). The simulations were performed for liquid binders of different viscosities. The percentage of abrasion produced by the model is compared with the experiments for different viscosities at time t = 60 seconds. The mass-averaged value of the diameter over the whole bed is taken as the final diameter of the agglomerate. The difference in the mass between the initial and the final agglomerate is taken as the mass that has been abraded. The conditions of the simulation setup are presented in the Table 4.3.

Table 4.3: Properties of fluidized bed for coke-binder simulations

Bed Height (initial)	0.15 m
Particle Diameter	0.000140 m
Agglomerate Diameter	0.0067 m
Agglomerate Volume Fraction (Initial)	0.0001
Agglomerate Patching Dimensions	0.15 m x 0.01
Particulate Volume Fraction (Initial)	0.55
Liquid Content (% wt)	1%
Coordination Number	8
Liquid Viscosity	6.44, 9.79, 16.10, 64.7 10^{-3}N.s/m^2
Liquid Surface Tension	0.03 N/m

Contact Angle	0°

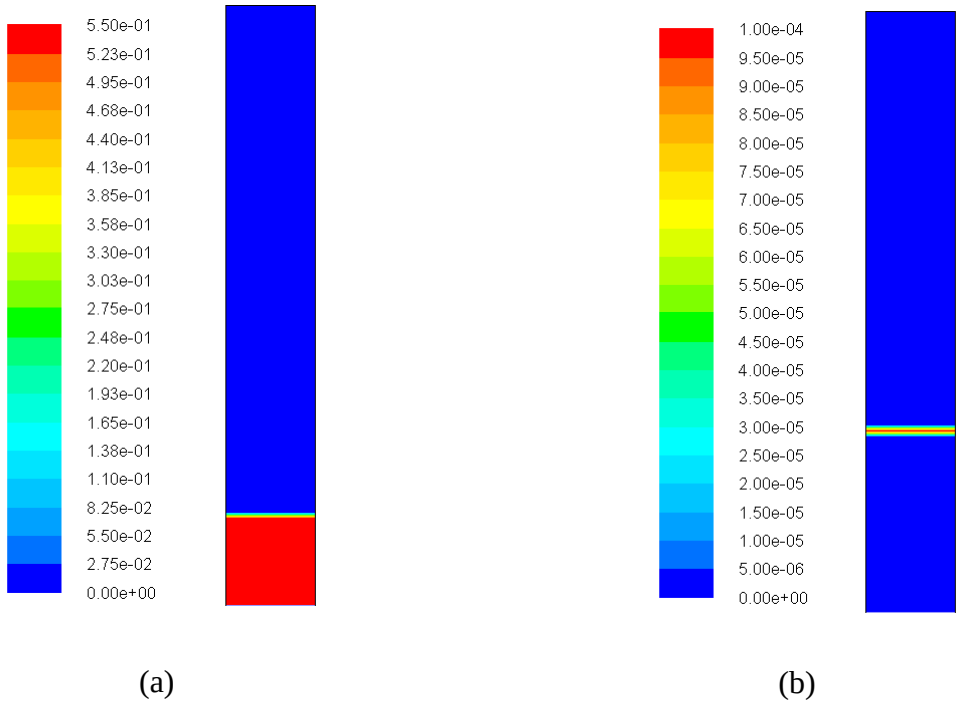

(a) (b)

Figure 4.3: Contour of volume fraction of (a) primary particle phase before gas flows is on (t = 0 s), (b) initial agglomerate phase (t = 0 s)

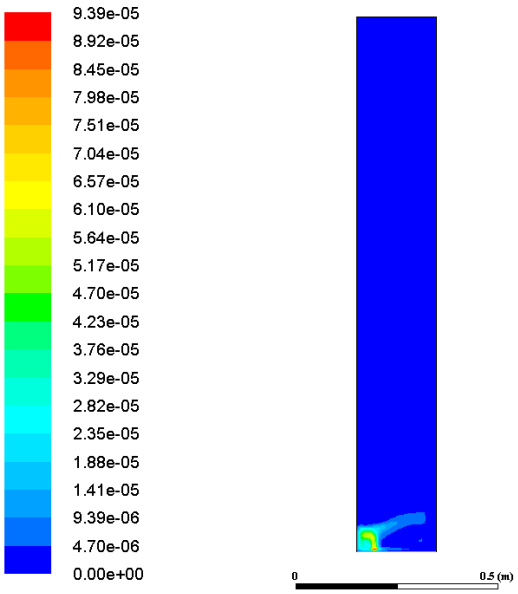

Figure 4.4 : Settling of the agglomerate in the coke-binder system at 60 s

4.2.1 Effect of Inlet Gas Velocity

Figures 4.5–4.8 show the abrasion prediction of the developed model in comparison with the experimental findings. Weber (14) repeated each experiment three to five times, and the average value of abrasion and standard deviation was reported. The vertical bars represent the standard deviation. The expectation is that the model would give a qualitatively good representation of the model and a quantitatively meaningful one. It has to be emphasized that the representation of the collision energy is simplified as the whole energy is considered to be transferred from the particle to the agglomerate. The experimental errors are significant as evidenced by the error bars. The hand-made agglomerate has non-homogeneities and stresses that are not accounted for in the model. The particles are assumed spherical and the bridges in between the particles are based on same size spheres. In reality the particles are not perfectly spherical. Also the particles are not mono-sized and the bridge strength expressions are based on interaction of spheres with

the same diameter. The agglomerate is assumed spherical, while it was cylindrical in the experiment. The model is entirely based on physics and there are no fitting parameters used. Also, only abrasion was considered, with no fragmentation modeled.

The computations predict a similar trend of abrasion with that reported in the experiments. Also, it can be seen that the slope is slightly decreasing with increasing velocity, despite the quadratic increase of the collision energy.. This is possible because the viscous energy shown in Equation (3.36) increases as well with increasing velocity, and hence the bond energy increases, resulting in less abrasion.

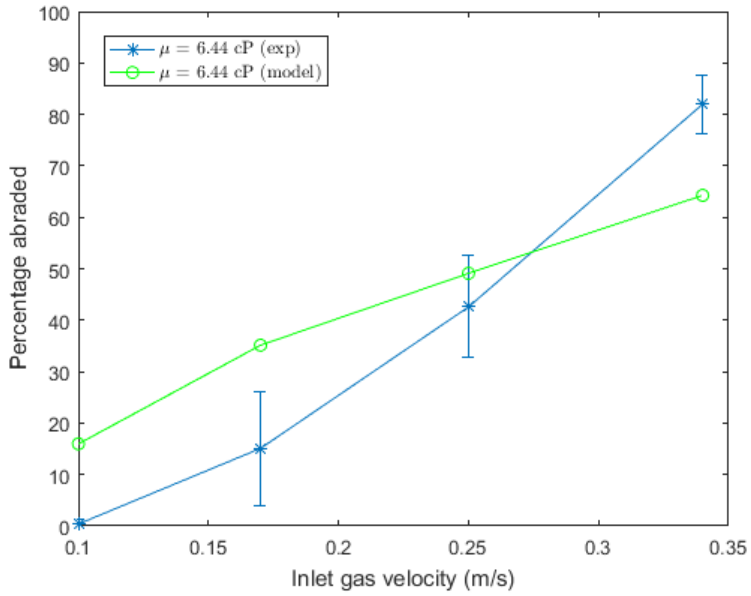

Figure 4.5 : Plot of abrasion percentage from experiment and the model prediction for 1% liquid content at μ = 6.44 cP

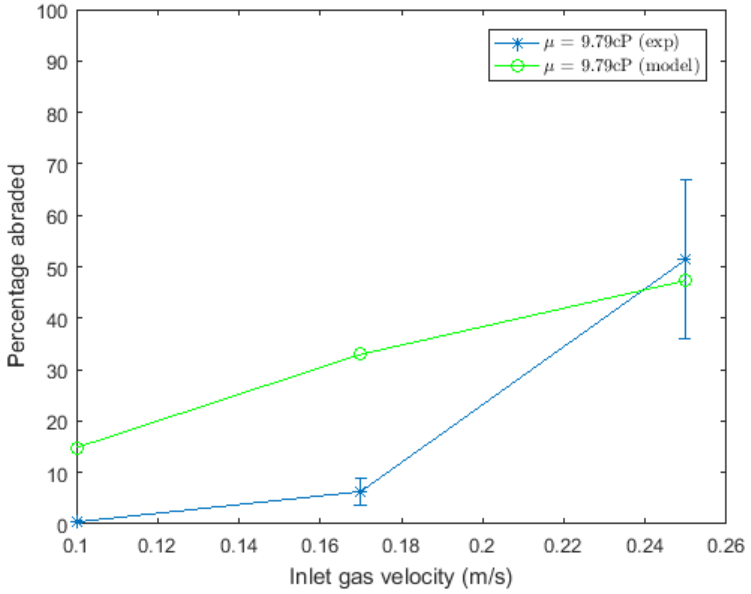

Figure 4.6 : Plot of abrasion percentage from experiment and model prediction for 1% liquid content at μ = 9.79 cP

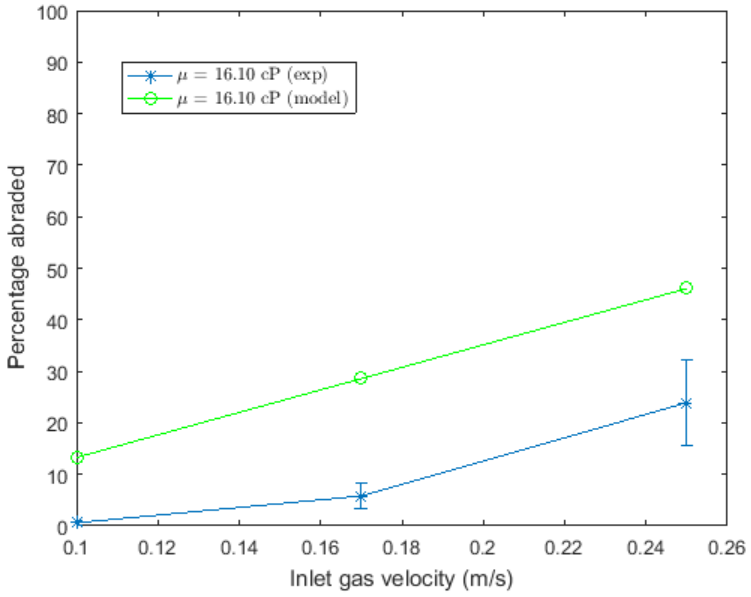

Figure 4.7 : Plot of abrasion percentage from experiment and model prediction for 1% liquid content at μ = 16.10 cP

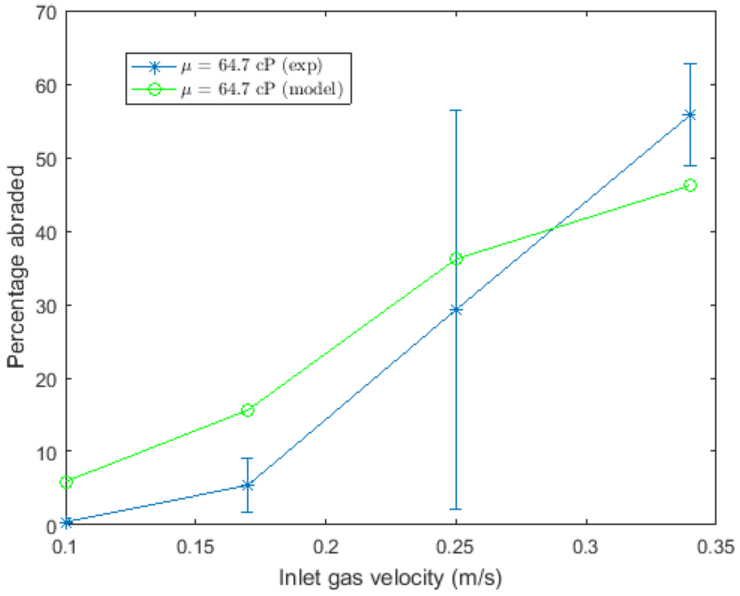

Figure 4.8 : Plot of abrasion percentage from experiment and model prediction for 1% liquid content at μ = 64.7 cP

Table 4.4: Number of fragments formed in experiment of Weber (14) for different conditions in coke-binder system

U (m/s)	$N_{fragments}$ (μ = 6.44 cP)	$N_{fragments}$ (μ = 9.79 cP)	$N_{fragments}$ (μ = 16.10 cP)	$N_{fragments}$ (μ = 64.7 cP)
0.10	1	1	1	1
0.17	29.2	12.6	9.0	4.2
0.25	33.5	34.4	27.0	24.8
0.34	23	N/A	N/A	47.0

4.2.2 Effect of Binder Viscosity

From Figures 4.9–4.11, it can be seen that the abrasion decreases with the increase in the binder viscosity, as expected. It is understood that with the increase in the binder viscosity, the pendular

bridges get stronger, and hence the amount of abrasion decreases. At U = 0.10 m/s, the collision energy is much lower, and hence the abrasion becomes negligible at higher viscosities. In the experiments, at U = 0.10 m/s, the percentage of abrasion ranges between 0.4% to 0.6%, and can therefore be considered negligible. From Figure 4.10, at U = 0.17 m/s, it can be seen that the model and the experiment share a similar trend. From Figure 4.11, it can be seen that the model predicts decreasing abrasion with increasing viscosity, but in the experiments the abrasion is noticed to increase with the increase of viscosity from 6.44 cP to 9.79 cP, which is counterintuitive. Considering the size of the error bars, this is most likely due to a variability of agglomerates produced in the laboratory.

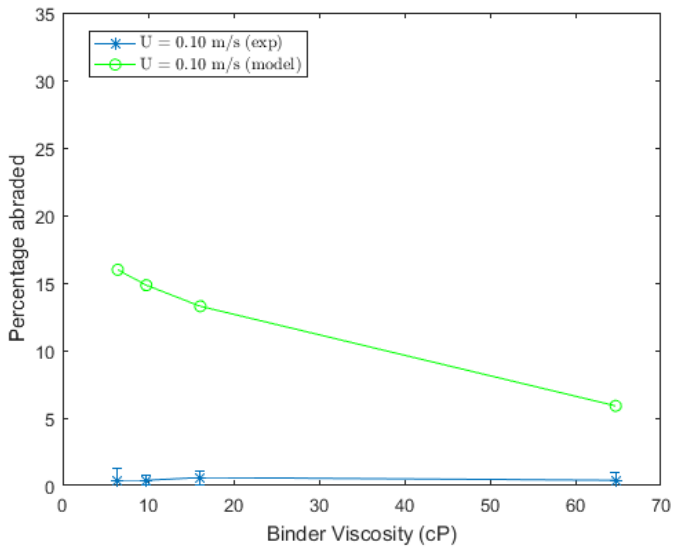

Figure 4.9: Plot of abrasion percentage from experiment and model prediction for 1% liquid content at U = 0.10 m/s

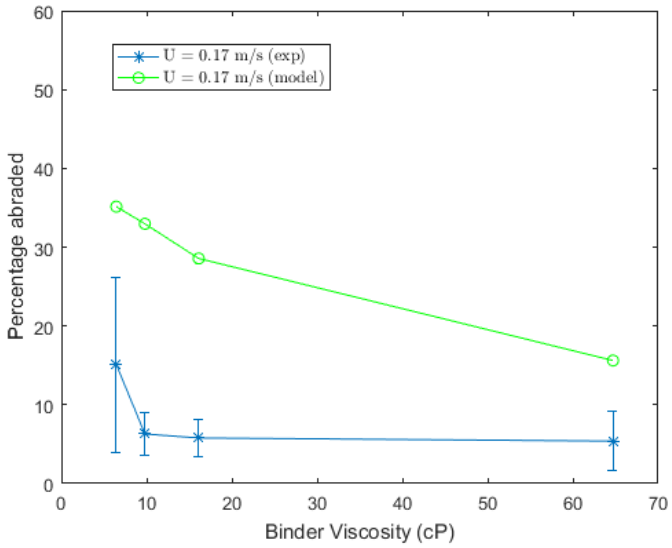

Figure 4.10 : Plot of abrasion percentage from experiment and model prediction for 1% liquid content at U = 0.17 m/s

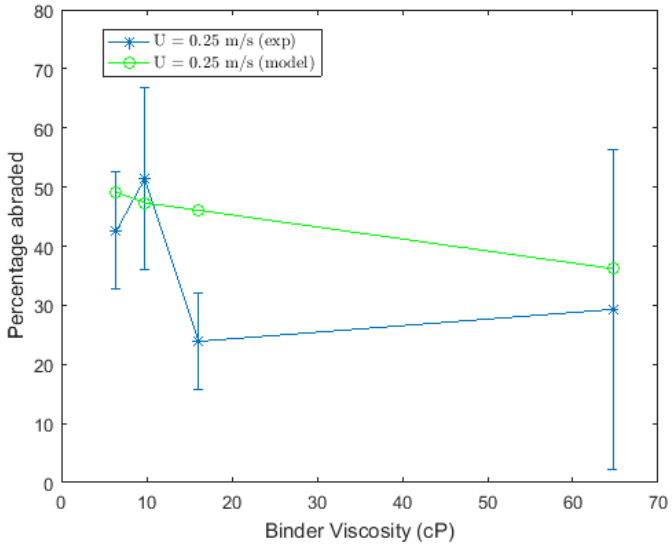

Figure 4.11: Plot of abrasion percentage from experiment and model prediction for 1% liquid content at U = 0.25 m/s

4.3 Comparison of Different Bed Material-Binder Setups

Similar to the coke-binder experiment, Weber et al. (56) performed experiments using glass beads of two different sizes and silica sand as the bed material. Water was used as the liquid binder. They also studied the effect of the contact angle on the stability of agglomerates. The untreated glass beads had a contact angle of 0º with water. The glass beads were treated in a solution of hexane and 5.10^{-3} % (by volume) trimethylsilyl N,N-dimethylcarbamate (Sigma–Aldrich, 98%). The contact angle of the treated glass beads with water was measured to be 65º using the Washburn technique proposed by Jackson et. al. (60). Similar to the coke-binder simulations, a lower value of agglomerate fraction was chosen and the area of patching was taken such that the volume of agglomerates in the simulation was equal to the volume of one agglomerate from the experiment. The conditions of the simulation setup are presented in Table 4.5.

Table 4.5 : Properties of fluidized bed for glass beads-binder and silica sand-binder simulations

Bed Height (initial)	0.15 m
Particle Diameter	0.000171 m, 0.000203 m, 0.000282 m
Agglomerate Diameter	0.0169 m
Agglomerate Volume Fraction (Initial)	0.001
Agglomerate Patching dimensions	0.15 m x 0.016
Particulate Volume Fraction (Initial)	0.55
Liquid content (% wt)	1%
Coordination number	8
Liquid Viscosity	0.000894 N.s/m^2
Liquid Surface Tension	0.07 N/m
Contact Angle	0°, 65°

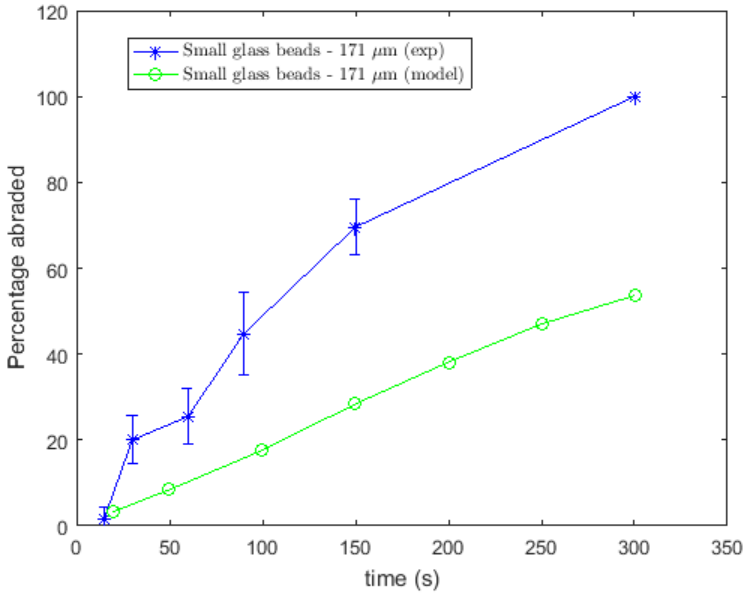

Figure 4.12 : Comparison of abraded percentages of experiment and model for 1% liquid content agglomerate for a small glass-beads system (untreated, contact angle = 0°)

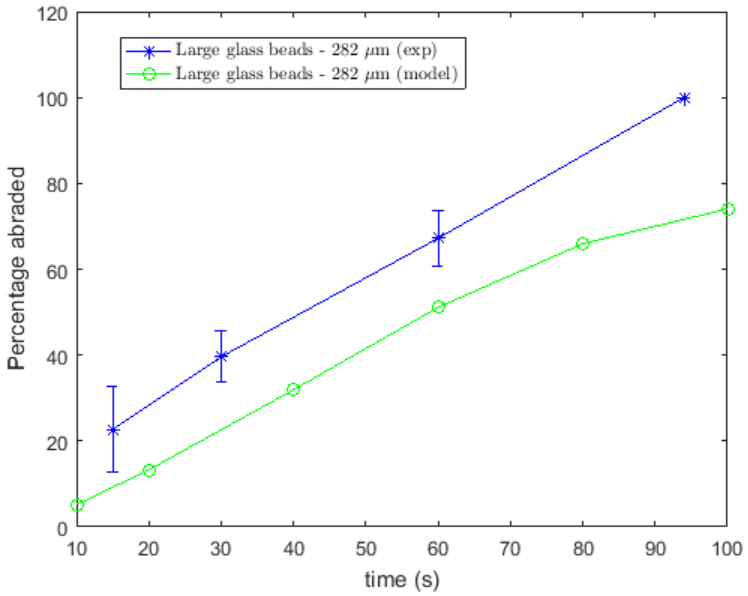

Figure 4.13 : Comparison of abrasion percentages of experiment and model for 1% liquid content agglomerate for a large glass-beads system (untreated, contact angle = 0°)

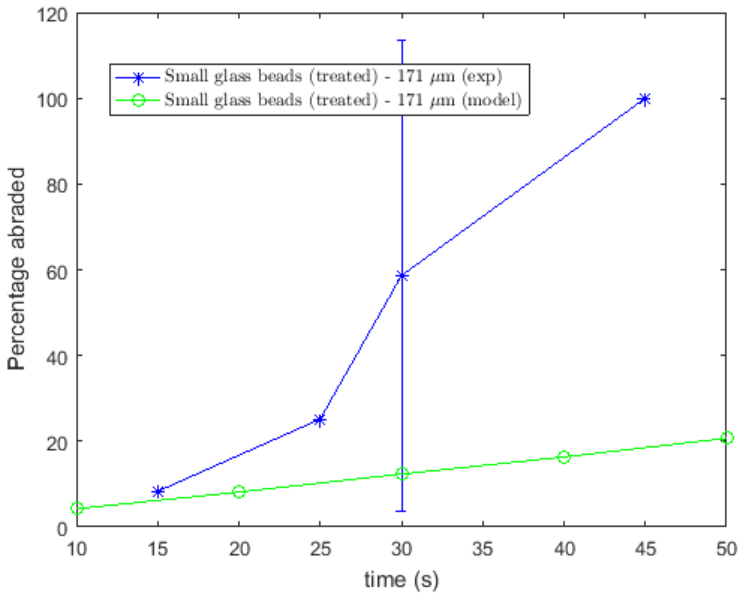

Figure 4.14: Comparison of abrasion percentages of experiment and model for 1% liquid content agglomerate for a small glass-beads system (treated, contact angle = 65°)

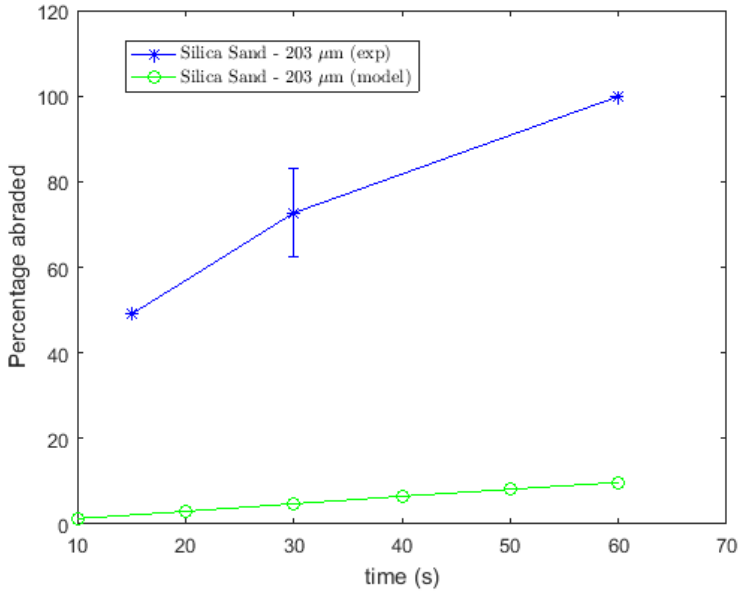

Figure 4.15: Comparison of abrasion percentages of experiment and model for 1% liquid content agglomerate silica sand system (untreated, contact angle = 0°)

From Figures 4.12–4.15, it can be seen that the model predicts the trend in the abrasion with time similar to the experiments. However, there is a quantitative difference in the percentage of abrasion between the experiments and the model. One of the possible reasons might be the absence of fragmentation in the model. Weber (56) in her work reported that the agglomerates broke into many fragments.

From the expression of the momentum exchange coefficient, K_{ls}, in Equation (3.22), it can be seen that the solid-solid drag decreases with the increase in the diameter of the agglomerate. With fragmentation in the experiments, the diameter of the agglomerate fragments drops, resulting in the increase in solid-solid drag. Hence, the fragments in the experiments are fluidized better and encounter more collision with the primary particles, compared to the model. In Figure 4.4, it can be seen that the agglomerate settles in the model, as the solid-solid drag is lower due to the bigger agglomerate size, which in turn is due to the lack of fragmentation. Also with fragmentation, the surface area exposed to the collision increases, leading to more erosion.

Table 4.6 compares model prediction between the glass beads-binder and silica sand setups. The percentage of underprediction, P_{up}, (difference in experimental results, R_{exp}, and model results, R_{model}) is calculated as

$$P_{up} = \frac{R_{exp} - R_{model}}{R_{exp}} \times 100 \quad \textbf{(4.1)}$$

and listed. Both setups have the same agglomerate size liquid binder and superficial gas velocity, and the results are compared at the point of complete abrasion in the experiments. It is interesting to see that the model predicts abrasion better in the glass-bead agglomerates case compared to

the silica agglomerates. It might be because the primary particles were assumed to be spherical in the model, whereas the silica particles used in the experiments were reported to be irregular in shape (14). The irregularity in silica particles can be seen from the microscopic image in Figure 4.2 (b). On the other hand, glass beads were spherical in the experiments, and the reason may be that the model predicts the abrasion better in the glass beads case. Also in the experiments, the irregular shape of the silica particles might have caused the agglomerates to be loose and to abrade faster (48).

Table 4.6: Comparison of model predictions between silica sand particles and glass beads setup

Particle type	Diameter μm	Contact Angle	Under prediction percentage
Small glass beads	171	0°	37%
Large glass beads	282	0°	65%
Treated small glass beads	171	65°	78%
Silica sand	203	0°	89%

4.4 Effect of Volume Fraction Patching

In the Eulerian-Eulerian model, the agglomerates are initially patched for a lower value of 0.0001 in the coke-binder simulations and a value of 0.001 in the glass beads setup. The volume fraction of the glass beads setup is higher than the coke setup because of the larger size of the glass bead agglomerate compared to the coke agglomerates. The volume of patch is chosen such that the total volume of the agglomerate phase in the setup is equal to the volume of one agglomerate used in the experiments. These very low values of volume fraction are chosen to

represent the single agglomerate used in the experiments by ensuring negligible interactions between the agglomerates in the model. The effect of the volume of patches on the abrasion is examined to determine whether the assumption to replace an agglomerate with the volume fraction patches is reasonable.

Table 4.7 : Comparison of fraction abraded for different volume fraction patching with viscosity of μ=6.44 cP in coke-binder setup

Velocity (m/s)	Fraction abraded V_p (0.0001)	Volume Fraction (0.0002)		Volume Fraction (0.0003)	
		Fraction abraded	% change	Fraction abraded	% change
0.10	0.1598	0.1537	- 3.81	0.1521	- 4.8
0.17	0.3515	0.3489	- 0.73	0.3526	0.32
0.25	0.4912	0.4809	- 1.99	0.4989	1.44
0.34	0.6429	0.6312	- 1.89	0.6371	- 0.90

From Table 4.7, it can be concluded that the value of volume fraction patching of the agglomerate does not have a significant effect on the abrasion of the agglomerates. For lower velocities, the abrasion is less for higher volume fraction. This might be caused by settling occurring faster at a lower superficial velocity.

4.5 Effect of Fluctuation Velocity

Previously, we had assumed that collisions between the particles and agglomerates took place due to differences in mean velocity. That is, the influence of the fluctuating part of the velocity component was neglected. This assumption will be examined further in this section. The

fluctuating velocity does not have a specific direction and is considered to have a Gaussian distribution (61). While it might be possible to rigorously obtain a collision frequency expression that takes collisional velocity into account, this is a complex mathematical exercise that goes beyond the scope of this work. Instead, we evaluate the influence of the collisional velocity by estimating its potential impact on the collision frequency.

Goldschmidt (39) used a second order approximation to derive the collision frequency due to the fluctuation components using the mixture granular temperature as

$$\tilde{n}_{pa} = \pi\, n_p n_a\, g_{0,pa}\ \sigma_{pa}^3 \left[\frac{4}{\sigma_{NP}} \left(\frac{\theta_s}{\pi} \frac{m_a + m_p}{2\, m_a m_p} \right)^{\frac{1}{2}} - \frac{2}{3} (\nabla . \bar{u}_s) \right] \tag{4.2}$$

where σ_{pa} is the distance between the centers of colliding particles, and hence is $\frac{(d_p + d_a)}{2}$. Ignoring the divergence in the particulate velocity field, the final collision frequency expression due to the fluctuation in the field is

$$\tilde{n}_{NP} = \pi\, n_p n_a\, g_{0,pa} \left(\frac{d_p + d_a}{2} \right)^2 \left[4 \left(\frac{\theta_s}{\pi} \frac{m_a + m_p}{2\, m_a m_p} \right)^{\frac{1}{2}} \right] \tag{4.3}$$

The mixture granular temperature is calculated as

$$\theta_s = \frac{1}{n_s} \sum_{n=1}^{NP} n_n \theta_n \tag{4.4}$$

where θ_n is calculated as

$$\theta_n = \frac{1}{3} \langle C_n^2 \rangle \tag{4.5}$$

Hence, the value fluctuation component of velocity of a particular phase can be written as

$$\langle C_n \rangle = \sqrt{3\, \theta_n} \tag{4.6}$$

Equation (4.3) was derived by Goldschmidt (39) considering that the mean velocities of colliding phases are equal and the collisions are only due to their fluctuation components. In the current modeling, as the mean velocities are different for different phases, the collision frequency expression in Equation (4.3) cannot be used directly. The effect of the fluctuation velocity on the abrasion is examined to determine its influence on the current model. Two extreme cases are taken where the fluctuation velocity has the same and opposite directions, respectively, relative to the mean velocity. Hence, the total velocity for both cases for the particulate phase can be written as

$$\vec{v}_p^{+} = \vec{v}_p + \langle C_p \rangle \hat{v}_p \quad \textbf{(4.7)}$$

$$\vec{v}_p^{-} = \vec{v}_p - \langle C_p \rangle \hat{v}_p \quad \textbf{(4.8)}$$

where $\hat{v}_p$ denotes a unit vector along the direction of $\vec{v}_p$. The above velocity expressions were used to calculate the collision frequency and collision energy from Equation (3.7) and Equation (3.39)**Error! Reference source not found.**, respectively. The percentage of change in the fraction of the mass eroded at 60 seconds is evaluated for the cases using the above velocity values. The results are shown in Table 4.8.

Table 4.8 : Comparison of fraction abraded for the opposite direction fluctuation velocities for a viscosity of μ=6.44cP in coke-binder setup

Velocity (m/s)	Fraction abraded	v_p^{+}		v_p^{-}	
		Fraction abraded	% change	Fraction abraded	% change
0.10	0.1598	0.1634	2.25	0.1566	-1.95
0.17	0.3515	0.3623	3.09	0.3436	- 2.23
0.25	0.4912	0.5094	3.71	0.4763	- 3.03
0.34	0.6429	0.6698	4.19	0.6209	- 3.41

From Table 4.8, it can be seen that the fluctuation velocity from the granular temperature does not play a significant role in the abrasion model. Similar simulations were performed for other viscosity values, and they led to the same conclusion. Hence, it could be concluded that it is not necessary to include the fluctuation velocity in the integration of the collision frequency.

The model developed predicts qualitative trends well. The quantitative disagreement is significant but to be expected. The model is complex and entirely based on the physics of process without any empirical fitting coefficients. It has a predictive capability because it reproduces trends, and therefore the ability to compare different parameters and assess which ones would produce more agglomeration. There are a number of factors that could affect the results. The geometrical simplification of replacing the cylinder with a sphere is likely to produce differences. Fragmentation has been ignored, and it is likely the most important cause of the under-prediction. Also, very importantly, the experiments were not reproducible and had very large error bars resulting most likely from imperfections in making the agglomerates, which could cause faster abrasion.

4.6 Fragmentation

Ideas on modeling fragmentation and defining fragmentation time scales are suggested here.

4.6.1.1 Fragmentation Modeling

Though the collision of individual particles with the agglomerates can cause destruction of agglomerates through the process of abrasion, there can be other processes that degrade the agglomerates. Fragmentation is one such process, and modeling it is important to enable the

simulation of the complete agglomeration process. In the following, a fragmentation model is proposed.

The solid drag force is large enough to lift the particles, which results in shear across the agglomerates, as shown in Figure 4.16. For fragmentation to be successful, all the bonds in the failure plane need to be broken, and hence the modeling is based on the strength of the planes, in contrast to erosion modeling where the modeling depends on individual bond strengths.

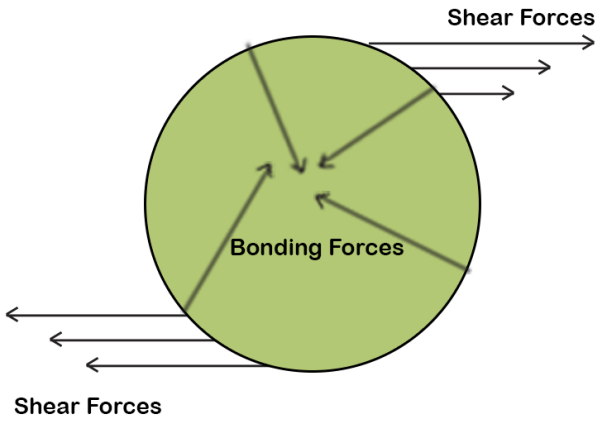

Figure 4.16: Shear forces on agglomerate caused by solid-solid drag

In the abrasion model, the probability term was defined in terms of the breakage energy of bonds as

$$P_{bond} = e^{-\frac{E_b}{E_c}} \quad \textbf{(4.9)}$$

Similarly, the probability term for the fragmentation model can be defined based on the shear due to drag, τ, and the shear strength of the agglomerate, σ. The shear strength of an agglomerate is defined as the shear needed for a failure to occur at the central plane of the agglomerate.

$$P_{fr} = e^{-\frac{\sigma}{\tau}} \tag{4.10}$$

where σ denotes the shear strength of the central plane of the agglomerate and τ denotes the shear across the agglomerate due to fluid or solid interaction. The biggest challenge in the development of the model is the time scale of the fragmentation (or the fragmentation frequency). As discussed earlier, Feng et al. (30) used a time scale based on the turbulent energy dissipation rate and kinematic viscosity as

$$t_{Xiao} = \sqrt{\frac{\epsilon_t}{\upsilon}} \tag{4.11}$$

where ϵ_t and υ are the turbulent energy dissipation rate and kinematic viscosity of the fluid, respectively. The developed model needed a scaling factor of the order of 10^{-3} to match the experiments. One of the main disadvantages of this type of time-scaling method is that experimental data are always needed to determine the fitting factor and it is system specific. Hence, it cannot be applied across a wide range of applications or used to predict fragmentation in a process.

One of the well-known models was developed by Moreno et al. (28) who proposed a mechanistic model that estimates the breakage of agglomerates during wall collisions. It assumes that the kinetic energy is proportional to the number of bonds broken, and the model depends on the impact velocity of the agglomerate with the wall, elastic modulus of the particles of the agglomerate, particle diameter and density, and the interface energy. In recent years, Moreno and

Ghadiri's in-built model in ANSYS Fluent has been used for modeling breakage (14, 62, 63) based on elasticity modulus (E_m) and interface energy (Γ). Fluent (64) incorporates the Ghadiri model into the population balance model (PBM) by adapting terms from it and defining the breakage kernel, f_b, as

$$f_b = \frac{\rho_p E^{2/3}}{\Gamma^{5/3}} V_p^2 d_p^{5/3} \quad \textbf{(4.12)}$$

4.6.1.2 Bond Breakage Time

Time scales for the individual bond breakages can be calculated using the equations from Pitois et al. (47) to calculate the time taken for an individual bond to break, t_b. Two different approaches can be used to calculate the bond breakage time.

4.6.1.2.1 Bond Breakage Time (approximate)

The bond breakage time can be approximated using the rupture distance and initial relative velocity of spheres, v_r, as

$$t_b = \frac{D_{rupt}^s}{v_r} \quad \textbf{(4.13)}$$

4.6.1.3 Time Scale of Fragmentation

The fragmentation time, t_{fr}, depends on the individual bond breakage time, t_b, and the total number of bonds broken and can be expressed as

$$t_{fr} = t_b \times N_{fr} \quad \textbf{(4.14)}$$

where N_{fr} denotes the number of bonds in the fragmentation plane. The fragmentation plane depends upon the external shear forces and internal bonding forces.

4.6.1.4 Fragmentation Frequency

The frequency of fragmentation, f_{fr}, can be written using the fragmentation probability, P_{fr}, and fragmentation time, t_{fr}, as

$$f_{fr} = \frac{P_{fr}}{t_{fr}} \tag{4.15}$$

The implementation of the fragmentation model is proposed for future work. This proposed fragmentation model can be combined with erosion to define a complete destruction mechanism in fluidized beds.

Chapter 5: Summary, Contribution, and Future Work

This chapter contains the summary of the results obtained from the developed model and the discussion on its comparison with the experimental data. Recommendations on the future work are also discussed.

5.1 Summary and Contributions

1 – A novel model based on the kinetic theory of granular flows (KTGF) was developed that predicts the abrasion of agglomerates in fluidized beds based on the proposed kernels for the frequency of abrasion.

2 – The model was used to predict abrasion for different superficial gas velocities, liquid, and granular properties. The results were compared with results from the lab-scale experiments performed by Weber (57) at the University of Western Ontario. The model predicted correctly the trends in the behavior of agglomerates with changing liquid properties and changing superficial gas velocities observed in the experiments. The predicted trends in the behavior of agglomerates with changing liquid properties and changing superficial gas velocities agreed with those observed during the experiments. The model in the coke-viscous binder over-predicted the amount of abrasion compared to the experiments. It is interesting to note this over-prediction while the glass beads-water case is under-predicted. It is not clear what the cause of this result is but it might be of interest to observe that the first case is viscous dominated while the second is more capillary dominated. In the case of the glass beads-water case, the model under-predicts abrasion. Possible reasons for the difference in results might be due to the absence of fragmentation and the assumption that the agglomerates are spherical. In the experiments, it was reported that fragmentation occurs. With fragmentation, the agglomerates fluidize better as

their size becomes smaller. Also due to the fragmentation in experiments, the overall surface area of the agglomerates available for interaction increases, leading to more abrasion. In the experiments, the cylindrical agglomerates were laboratory made, and it might be possible that the agglomerates had internal property variations which caused more fragmentation. The presence of these variations is supported by the large relative standard deviation observed for the experimental results. Also cylindrical structures have stress points at the corner edges compared to spherical structures, which could be another reason for more abrasion and fragmentation in the experiments. Also the model proposed is entirely based on the physics of the process and has no empirical adjustment coefficients, and therefore it cannot be expected to have a very close quantitative agreement with any particular set of experimental data.

3 – The robustness of the model was also tested by altering the volume fraction patch of the agglomerate that showed no significant change in abrasion.

4- The influence of fluctuating velocity on abrasion was also investigated and no significant change was observed between the two extreme values.

4 – A mechanistic model for fragmentation is proposed in the last chapter. This model is a novel approach that differs from most of the models in the literature due to the addition of a time scale for fragmentation based on the liquid bond rupture time.

5.2 Future Work and Recommendations

One of the main advantages of using a mechanistic model is that it could be extended to different processes and it does not depend on experimental results for closure. Hence a model that is a combination of the abrasion and fragmentation models could be a powerful tool to predict and understand the degradation process of agglomerates, which could be useful to improve the design

and development of reactors. The effect of constant parameters used in the model such as coordination number, restitution coefficient, etc., on abrasion should be investigated. Also, in an industrial reactor, the growth of agglomerates occurs simultaneously with destruction. Therefore, the abrasion and fragmentation models can be combined with a suitable agglomeration model to predict the behavior of agglomerates. In view of the importance of agglomeration in many processes, a physically based predictive model would lead to considerable progress in the understanding of process and improved design and operation.

References

1. Board CNE. Canada's Energy Future 2013 - Energy Supply and Demand Projections to 2035 - An Energy Market Assessment.

2. House PK, Saberian M, Briens CL, Berruti F, Chan E. Injection of a liquid spray into a fluidized bed: particle-liquid mixing and impact on fluid coker yields. Industrial & engineering chemistry research. 2004;43(18):5663-9.

3. Mishra B, Thornton C. Impact breakage of particle agglomerates. International Journal of Mineral Processing. 2001;61(4):225-39.

4. Landau LD, Kosevich A, Pitaevskii LP, Lifshitz EM. Theory of elasticity. 1986.

5. Seville J, Willett C, Knight P. Interparticle forces in fluidisation: a review. Powder technology. 2000;113(3):261-8.

6. Anderson TB, Jackson R. Fluid mechanical description of fluidized beds. Equations of motion. Industrial & Engineering Chemistry Fundamentals. 1967;6(4):527-39.

7. Iveson SM, Litster JD, Hapgood K, Ennis BJ. Nucleation, growth and breakage phenomena in agitated wet granulation processes: a review. Powder technology. 2001;117(1):3-39.

8. Schæfer T, Mathiesen C. Melt pelletization in a high shear mixer. IX. Effects of binder particle size. International journal of pharmaceutics. 1996;139(1):139-48.

9. Iveson S, Litster J. Growth regime map for liquid-bound granules. American Institute of Chemical Engineers AIChE Journal. 1998;44(7):1510.

10. McDougall S, Saberian M, Briens C, Berruti F, Chan E. Effect of liquid properties on the agglomerating tendency of a wet gas–solid fluidized bed. Powder technology. 2005;149(2):61-7.

11. Rajniak P, Mancinelli C, Chern R, Stepanek F, Farber L, Hill B. Experimental study of wet granulation in fluidized bed: impact of the binder properties on the granule morphology. International journal of pharmaceutics. 2007;334(1):92-102.

12. Knight P, Johansen A, Kristensen H, Schaefer T, Seville J. An investigation of the effects on agglomeration of changing the speed of a mechanical mixer. Powder Technology. 2000;110(3):204-9.

13. Watano S, Sato Y, Miyanami K, Murakami T, Ito Y, Kamata T, et al. Scale-Up of Agitation Fluidized Bed Granulation. I. Preliminary Experimental Approach for Optimization of Process Variables. Chemical and pharmaceutical bulletin. 1995;43(7):1212-6.

14. Weber S, Briens C, Berruti F, Chan E, Gray M. Stability of agglomerates made from fluid coke at ambient temperature. Powder technology. 2011;209(1):53-64.

15. Vonk P, Guillaume C, Ramaker J, Vromans H, Kossen N. Growth mechanisms of high-shear pelletisation. International journal of pharmaceutics. 1997;157(1):93-102.

16. Pietsch W. An interdisciplinary approach to size enlargement by agglomeration. Powder technology. 2003;130(1):8-13.

17. Sherrington P, Oliver R. Granulation monograph (chapter 3). Powder Science and Technology London: Heyden. 1981.

18. Washino K, Miyazaki K, Tsuji T, Tanaka T. A new contact liquid dispersion model for discrete particle simulation. Chemical Engineering Research and Design. 2016.

19. Gidaspow D. Multiphase flow and fluidization: continuum and kinetic theory descriptions: Academic press; 1994.

20. Sinclair JL. Hydrodynamic modeling. In: Grace JR, Avidan AA, Knowlton TM, editors. Circulating fluidized beds: Chapman & Hall; 1997. p. 149-80.

21. Deen N, Annaland MVS, Van der Hoef M, Kuipers J. Review of discrete particle modeling of fluidized beds. Chemical Engineering Science. 2007;62(1):28-44.

22. Enwald H, Peirano E, Almstedt A-E. Eulerian two-phase flow theory applied to fluidization. International Journal of Multiphase Flow. 1996;22:21-66.

23. Van Wachem B, Almstedt A-E. Methods for multiphase computational fluid dynamics. Chemical Engineering Journal. 2003;96(1):81-98.

24. Esmaili E, Mahinpey N. Adjustment of drag coefficient correlations in three dimensional CFD simulation of gas–solid bubbling fluidized bed. Advances in Engineering Software. 2011;42(6):375-86.

25. Gidaspow D, Bezburuah R, Ding J. Hydrodynamics of circulating fluidized beds: kinetic theory approach. Illinois Inst. of Tech., Chicago, IL (United States). Dept. of Chemical Engineering, 1991.

26. Hemati M, Cherif R, Saleh K, Pont V. Fluidized bed coating and granulation: influence of process-related variables and physicochemical properties on the growth kinetics. Powder Technology. 2003;130(1):18-34.

27. Kendall K. Agglomerate Strength. Powder Metallurgy. 1988;31(1):28-31.

28. Moreno-Atanasio R, Ghadiri M. Mechanistic analysis and computer simulation of impact breakage of agglomerates: effect of surface energy. Chemical engineering science. 2006;61(8):2476-81.

29. Subero J, Ning Z, Ghadiri M, Thornton C. Effect of interface energy on the impact strength of agglomerates. Powder technology. 1999;105(1):66-73.

30. Feng X, Xiao-Yan L. Modelling the kinetics of aggregate breakage using improved breakage kernel. Water Science & Technology. 2008;57(1).

31. Shamlou AA, Liu Z, Yates J. Hydrodynamic influences on particle breakage in fluidized beds. Chemical Engineering Science. 1990;45(4):809-17.

32. Syamlal M, Rogers W, O'Brien TJ. MFIX documentation: Theory guide. National Energy Technology Laboratory, Department of Energy, Technical Note DOE/METC-95/1013 and NTIS/DE95000031. 1993.

33. Wen C, Yu Y, editors. Mechanics of fluidization. Chem Eng Prog Symp Ser; 1966.

34. Ergun S. Fluid flow through packed columns. Chem Eng Prog. 1952;48:89-94.

35. Savage S, Jeffrey D. The stress tensor in a granular flow at high shear rates. Journal of Fluid Mechanics. 1981;110:255-72.

36. Jenkins J, Savage S. A theory for the rapid flow of identical, smooth, nearly elastic, spherical particles. Journal of Fluid Mechanics. 1983;130:187-202.

37. Ding J, Gidaspow D. A bubbling fluidization model using kinetic theory of granular flow. AIChE Journal. 1990;36(4):523-38.

38. Chapman S, Cowling TG. The mathematical theory of non-uniform gases: an account of the kinetic theory of viscosity, thermal conduction and diffusion in gases: Cambridge University Press, Cambridge, UK; 1970.

39. Goldshmidt M. Hydrodynamic modelling of fluidized bed granulation. Twente University. 2001.

40. Lun C, Savage SB, Jeffrey D, Chepurniy N. Kinetic theories for granular flow: inelastic particles in Couette flow and slightly inelastic particles in a general flowfield. Journal of Fluid Mechanics. 1984;140:223-56.

41. Ogawa S, Umemura A, Oshima N. On the equations of fully fluidized granular materials. Zeitschrift für angewandte Mathematik und Physik ZAMP. 1980;31(4):483-93.

42. Dartevelle S. Numerical modeling of geophysical granular flows: 1. A comprehensive approach to granular rheologies and geophysical multiphase flows. Geochemistry, Geophysics, Geosystems. 2004;5(8).

43. Kolev NI, Kolev N. Multiphase flow dynamics 2: Springer; 2005.

44. Gidaspow D, Lu H. Equation of state and radial distribution functions of FCC particles in a CFB. AIChE Journal. 1998;44(2):279-93.

45. Syamlal M. The particle-particle drag term in a multiparticle model of fluidization. EG and G Washington Analytical Services Center, Inc., Morgantown, WV (USA), 1987.

46. Kusters KA, Pratsinis SE, Thoma SG, Smith DM. Ultrasonic fragmentation of agglomerate powders. Chemical Engineering Science. 1993;48(24):4119-27.

47. Pitois O, Moucheront P, Chateau X. Liquid bridge between two moving spheres: An experimental study of viscosity effects. Journal of Colloid and Interface Science. 2000;231(1):26-31.

48. Lian G, Thornton C, Adams MJ. A theoretical study of the liquid bridge forces between two rigid spherical bodies. Journal of Colloid and Interface Science. 1993;161(1):138-47.

49. Darabi P, Pougatch K, Salcudean M, Grecov D, editors. Numerical Studies of Stretching Liquid Bridges between Two Solid Spherical Particles with Different Contact Angles. ASME International Mechanical Engineering Congress and Exposition; 2010.

50. Darabi P. Mathematical modeling of interaction of wet particles and application to fluidized beds [PhD Thesis]: The University of British Columbia (Vancouver); 2011.

51. Darabi P, Pougatch K, Salcudean M, Grecov D. A novel coalescence model for binary collision of identical wet particles. Chemical Engineering Science. 2009;64(8):1868-76.

52. Benyahia S. Analysis of model parameters affecting the pressure profile in a circulating fluidized bed. AIChE Journal. 2012;58(2):427-39.

53. Rajniak P, Stepanek F, Dhanasekharan K, Fan R, Mancinelli C, Chern R. A combined experimental and computational study of wet granulation in a Wurster fluid bed granulator. Powder Technology. 2009;189(2):190-201.

54. Shamlou PA, Stavrinides S, Titchener-Hooker N, Hoare M. Growth-independent breakage frequency of protein precipitates in turbulently agitated bioreactors. Chemical Engineering Science. 1994;49(16):2647-56.

55. Pougatch K. Mathematical modelling of gas and gas-liquid jets injected into a fluidized bed [PhD Thesis]: The University of British Columbia (Vancouver); 2011.

56. Weber S, Briens C, Berruti F, Chan E, Gray M. Agglomerate stability in fluidized beds of glass beads and silica sand. Powder technology. 2006;165(3):115-27.

57. Weber SC. Agglomerate stability in fluidized beds [PhD Thesis]: The University of Western Ontario; 2009.

58. Ahmadi Motlagh AH. CFD simulation of two-and three-phase flow in FCC reactors: The University of British Columbia (Vancouver); 2015.

59. Darabi P, Pougatch K, Salcudean M, Grecov D. Agglomeration of bitumen-coated coke particles in fluid cokers. International Journal of Chemical Reactor Engineering. 2010;8(1).

60. Jackson P, Hunt J, Doherty P, Cannon A, Gilson P. Hydrophilicity of 3-D biomaterials: the Washburn equation. Journal of Materials Science: Materials in Medicine. 2004;15(4):507-11.

61. Carnahan NF, Starling KE. Equation of state for nonattracting rigid spheres. The Journal of Chemical Physics. 1969;51(2):635-6.

62. Li F, Briens C, Berruti F, McMillan J. Particle attrition with supersonic nozzles in a fluidized bed at high temperature. Powder technology. 2012;228:385-94.

63. Mawson RA. Bubble coalescence and breakup modeling for computing mass transfer coefficient [Master's Thesis]: Utah State University; 2012.

64. Inc. F. Fluent 16 User's Guide. 2015.